

THE IMPACT OF LOCAL GEOMETRY AND BATCH SIZE ON THE CONVERGENCE AND DIVERGENCE OF STOCHASTIC GRADIENT DESCENT*

VIVAK PATEL[†]

Abstract. Stochastic small-batch (SB) methods, such as mini-batch Stochastic Gradient Descent (SGD), have been extremely successful in training neural networks with strong generalization properties. In the work of Keskar et. al (2017), an SB method’s success in training neural networks was attributed to the fact it converges to flat minima—those minima whose Hessian has only small eigenvalues—while a large-batch (LB) method converges to sharp minima—those minima whose Hessian has a few large eigenvalues. Commonly, this difference is attributed to the noisier gradients in SB methods that allow SB iterates to escape from sharp minima. While this explanation is intuitive, in this work we offer an alternative mechanism. In this work, we argue that SGD escapes from or converges to minima based on a deterministic relationship between the learning rate, the batch size, and the local geometry of the minimizer. We derive the exact relationships by a rigorous mathematical analysis of the canonical quadratic sums problem. Then, we numerically study how these relationships extend to nonconvex, stochastic optimization problems. As a consequence of this work, we offer a more complete explanation of why SB methods prefer flat minima and LB methods seem agnostic, which can be leveraged to design SB and LB training methods that have tailored optimization properties.

Key words. Stochastic Gradient Descent, Local Geometry, Batch Size, Learning Rate, Convergence, Divergence

AMS subject classifications. 90C15, 90C30

1. Introduction. Stochastic small-batch (SB) methods, such as stochastic gradient descent (SGD), have been extremely successful in training neural networks with strong generalization properties as demonstrated by the many applications of the algorithm in deep learning [2, 3, 5]. In the work of Keskar et. al. [4], SB methods and large-batch (LB) methods (e.g., Gradient Descent) were studied in order to understand the reasons why these SB methods have greater success at training generalizable neural networks in comparison to LB methods. The authors observed the following: “The lack of generalization ability [of neural networks trained by large-batch methods] is due to the fact that large-batch methods tend to converge to sharp minimizers of the training function. These minimizers are characterized by a significant number of large positive eigenvalues in [the Hessian at the minimizer], and tend to generalize less well. In contrast, small-batch methods converge to flat minimizers characterized by having numerous small eigenvalues of [the Hessian at the minimizer]. We have observed that the loss function landscape of deep neural networks is such that large-batch methods are attracted to regions with sharp minimizers and that, unlike small-batch methods, are unable to escape basins of attraction of these minimizers” [4].

The pervading, de facto explanation for this phenomenon is intuitive: because the difference between SB and LB methods is that SB methods have greater variability, it must be an SB method’s variability that allows it to escape sharp minima. However, this explanation does not fully address two other observations made by Keskar et. al. [4].

First, Keskar et. al. “conclude this section by noting that the sharp minimiz-

*March 26, 2025.

Funding: This work was funded by U.S. Department of Energy, Office of Science, under Contract No. DE-AC02-06CH11357.

[†]Dept. of Statistics, University of Chicago, Chicago, IL (vp314@uchicago.edu, vivakpatel.org).

ers identified in our experiments do not resemble a cone, i.e., the function does not increase rapidly along all (or even most) directions. By sampling the loss function in a neighborhood of [large-batch method] solutions, we observe that it rises steeply only along a small dimensional subspace (e.g. 5% of the whole space); on most other directions, the function is relatively flat” [4]. Indeed, if only the variability modulates which type of minimizer SB methods should find, then we should expect, just by chance, that some of the SB methods get stuck in sharp minima. However, none of the SB methods presented ended up in sharp minima.

Second, Keskar et. al. attempted to use several approaches to improve the generalizability of LB methods: “These approaches include data augmentation, conservative training and adversarial training. Our preliminary findings show that these approaches help reduce the generalization gap but still lead to relatively sharp minimizers and as such, do not completely remedy the problem” [4]. Two of these three approaches, in some sense, add variability to the gradient steps; however, the LB methods still converge to sharp minima despite this added variability. In light of these two observations, it seems that variability is not enough to explain why SB methods converge to flat minima, and LB methods are agnostic.

In this work, we mathematically and numerically argue that SGD’s preference for certain minima is described by an alternative mechanism: SGD’s divergence from or convergence to a minimizer depends on the deterministic interaction between the learning rate, batch-size and the expected local geometry of the objective function at the minimizer.

In [section 2](#), we state precise mathematical relationships between SGD’s divergence from or convergence to a minimizer and these previously enumerated quantities for the fundamental case of the quadratic problem. Beyond the precise description of when SB and LB methods diverge from or converge to a minimizer, the results of [section 2](#) have important practical implications for designing optimal sampling schemes and have important methodological contributions as they bring SGD and Gradient Descent under a uniform theoretical treatment. In [section 3](#), we numerically study how well the results of [section 2](#) extend to a contrived, nonsmooth, nonconvex stochastic optimization problem in two dimensions. Our numerical experiments show that the intuition and the mathematical relationships translate well to this nonconvex case. In [section 4](#), we numerically study a nonconvex optimization problem, first introduced in the neural network literature, that has a rich surface structure, but also has a tractable analytical form. Again, we show that the intuition and relationships from the results of [section 2](#) also translate to this more realistic problem. In [section 5](#), we summarize the main contributions of this work and discuss their implications for designing learning rates and choosing batch sizes to guarantee different types of convergence behavior.

2. The Quadratic Problem. First, we define the quadratic sums problems that we will use to study SGD.

PROBLEM 1 (Homogeneous Quadratic Sums). *Fix $\beta^* \in \mathbb{R}^d$. Let $Q_1, \dots, Q_N \in \mathbb{R}^{d \times d}$ be symmetric, positive semi-definite, and $r_1, \dots, r_N \in \mathbb{R}^d$ such that*

$$\beta^* \in \arg \min_{\beta} \frac{1}{2} \beta' Q_i \beta + r_i' \beta,$$

for $i = 1, \dots, N$. The quadratic sums problem is to solve

$$(1) \quad \min \sum_{i=1}^N \frac{1}{2} \beta' Q_i \beta + r_i' \beta.$$

The fact that β^* is a common minimizer for each of the components is generally unrealistic beyond consistent linear systems, some convex problems, and some deep neural networks. However, it is closely related to the following, more realistic problem, which we will also call the quadratic sums problem—an abuse of nomenclature that we will reconcile below.

PROBLEM 2 (Inhomogeneous Quadratic Sums). *Let $Q_1, \dots, Q_n \in \mathbb{R}^{d \times d}$ be symmetric and $r_1, \dots, r_N \in \mathbb{R}^d$ such that for each $i = 1, \dots, N$*

$$\frac{1}{2}\beta'Q_i\beta + r_i'\beta,$$

is bounded from below. The quadratic sums problem is to solve

$$(2) \quad \min \sum_{i=1}^N p_i \left(\frac{1}{2}\beta'Q_i\beta + r_i'\beta \right),$$

where p_i are positive valued and sum to one.

In order to reconcile the nomenclature, we will need some straightforward properties of [Problems 1](#) and [2](#).

LEMMA 3. *The objective function, (1), in [Problem 1](#) is equivalent to*

$$\frac{1}{2}(\beta - \beta^*)' \left[\sum_{i=1}^N Q_i \right] (\beta - \beta^*),$$

up to an additive constant, and, hence, is convex.

Proof. Since β^* is a solution to $Q_i\beta = -r_i$, then we can rewrite each component of (1), up to an additive constant, as $0.5(\beta - \beta^*)'Q_i(\beta - \beta^*)$. Hence, the objective is equal to, up to an additive constant, $0.5(\beta - \beta^*)' \left[\sum_{i=1}^N Q_i \right] (\beta - \beta^*)$. Since the Hessian of the objective is positive semi-definite, the objective function is convex. \square

LEMMA 4. *For $Q_1, \dots, Q_N, r_1, \dots, r_N$ as in [Problem 1](#) and for any positive constants a_1, \dots, a_N , a solution to*

$$\min \sum_{i=1}^N a_i \left[\frac{1}{2}\beta'Q_i\beta + r_i'\beta \right],$$

is also a solution to [Problem 1](#).

Proof. Just as for the original objective function, the weighted objective function, $\sum_{i=1}^N a_i \left[\frac{1}{2}\beta'Q_i\beta + r_i'\beta \right]$, is equal to $(\beta - \beta^*)' \left[\sum_{i=1}^N a_i Q_i \right] (\beta - \beta^*)$, up to an additive constant, and, consequently, it is also convex. Moreover, by convexity, for any

$$\tilde{\beta} \in \arg \min (\beta - \beta^*)' \left[\sum_{i=1}^N a_i Q_i \right] (\beta - \beta^*),$$

we must have $0 = (\tilde{\beta} - \beta^*)' \left[\sum_{i=1}^N a_i Q_i \right] (\tilde{\beta} - \beta^*)$. Since each $Q_i \succeq 0$ and $a_i > 0$, it follows that $(\tilde{\beta} - \beta^*)'Q_i(\tilde{\beta} - \beta^*) = 0$. Therefore, $\tilde{\beta}$ is also a minimizer to (1). \square

LEMMA 5. *In [Problem 2](#), for each $i = 1, \dots, N$, Q_i is positive semi-definite, and r_i is in the image space of Q_i .*

Proof. Suppose Q_i has a negative eigenvalue λ , and let v be a unit eigenvector corresponding to this eigenvalue. Then, for any α , $\frac{1}{2}\alpha^2 v' Q_i v + \alpha r_i' v = \frac{1}{2}\alpha^2 \lambda + \alpha r_i' v$, which goes to negative infinity for α sufficiently large in magnitude and positive. Hence, we have a contradiction since each component of the objective function is bounded from below.

Now, suppose r_i is not in the image space of Q_i . Then, we can write $r_i = v + w$ where w is the orthogonal projection of r_i onto the image space of Q_i and v is orthogonal to w . Then, for any α , $\frac{1}{2}\alpha^2 v' Q_i v + \alpha r_i' v = 0 + \alpha \|v\|_2^2$, which goes to negative infinity for α sufficiently large in magnitude and negative. Hence, we have a contradiction. \square

LEMMA 6. *Let $\beta^* = -\left(\sum_{i=1}^N p_i Q_i\right)^\dagger \left(\sum_{i=1}^N p_i r_i\right)$. Then the objective function, (2), in Problem 2, is equivalent to*

$$\frac{1}{2}(\beta - \beta^*)' \left[\sum_{i=1}^N p_i Q_i \right] (\beta - \beta^*),$$

up to an additive constant.

Proof. Let $\bar{Q} = \sum_{i=1}^N p_i Q_i$ and $\bar{r} = \sum_{i=1}^N p_i r_i$. Note that $(\beta - \beta^*)' \bar{Q} (\beta - \beta^*) = \beta' \bar{Q} \beta - 2\beta' \bar{Q} \beta^* + \beta^* \bar{Q} \beta^*$. Dropping the constant and noting that $\bar{Q} \beta^* = -\bar{r}$ (\bar{r} must be in the image space of \bar{Q} by the same reasoning as in Lemma 5), we have that $(\beta - \beta^*)' \bar{Q} (\beta - \beta^*) = \beta' \bar{Q} \beta + 2\beta' \bar{r}$. Replacing \bar{Q} and \bar{r} with their definitions and dividing by two recovers (2). \square

In light of Lemma 6, Problem 2 is a special case of Problem 1 when each component of the objective function has a common minimizer. Then, we can distinguish between Problems 1 and 2 by requiring that when a homogeneous minimizer exists, then the quadratic sums problem refers to Problem 1, and when no common minimizer exists, then the quadratic sums problem refers to Problem 2.

Now, in order to study SGD of a batch size k , which we refer to as SGD- k , on Problems 1 and 2, we will need to specify two more quantities that describe the geometry of the quadratic objective. Define $\bar{Q} = \sum_{i=1}^N p_i Q_i$ and $\bar{F} = \sum_{i=1}^N p_i Q_i \bar{Q} Q_i$, where, p_i are positive valued and sum to one. Then, the following property holds.

LEMMA 7. *Let Q_i be as in Problem 1 or Problem 2. If for some $x \in \mathbb{R}^d$, $x' \bar{Q} x = 0$ then $x' \bar{F} x = 0$.*

Proof. If $x = 0$ then this holds trivially. Suppose $x \neq 0$. If $x' \bar{Q} x = 0$ then, since $Q_i \succeq 0$ and $p_i \neq 0$, then $x' Q_i x = 0$ for each i . Hence, x is in the null space of each Q_i . So, $x' \bar{F} x = \sum_{i=1}^N p_i x' Q_i \bar{Q} Q_i x = 0$. \square

Furthermore, we will make use of the following assumption about the relationship between \bar{F} and \bar{Q} .

ASSUMPTION 8 (Moment Assumption). $\exists \gamma \geq 0$ such that $\bar{F} \succeq (1 + \gamma) \bar{Q}^3$.

There are two main benefits of Assumption 8. First, it allows for a uniform and, from our experience, more accurate characterization of the behavior of SGD- k for $k \in \mathbb{N} \cup \infty$. Second and more importantly, it ensures that our lower bound estimates of the error are non-negative. However, the condition in Assumption 8 is clearly counter-intuitive: from our usual experience with the Hölder's Inequality with vectors and functions, we should expect the opposite inequality to hold. This raises a question: for what collections $\{p_1, \dots, p_N\}$ and $\{Q_1, \dots, Q_N\}$, as described in Problems 1 and 2,

is [Assumption 8](#) always true? In the one-dimensional case, [Assumption 8](#) is equivalent to the variance of a random variable being non-negative. Also, this inequality is easily satisfied with $\gamma = 1$ for online linear regression problems whose features are mean-zero and normally distributed. While these claims do not constitute a guarantee that [Assumption 8](#) holds, because it is used in our arguments, we provide numerical evidence that this property holds generally in [Appendix A](#). Then, in [subsection 2.1](#), for [Problem 1](#), we state and prove a precise mathematical relationship between the learning rate, batch-size, and expected local geometry of the objective function in determining convergence to or divergence from a minimizer. In [subsection 2.2](#), we state a similar mathematical relationship for [Problem 2](#).

2.1. Mathematical Characterization for the Homogeneous Problem.

We now characterize when SGD- k diverges from a minimizer of [Problem 1](#) based on the batch-size, learning rate and local geometry of the equivalent objective function defined in [Lemma 4](#). This characterization follows a standard approach with the addition of a convex approximation and use of [Assumption 8](#) to derive a lower bound on the expected optimality gap. Before stating the essential steps, we must first define SGD- k .

DEFINITION 9 (SGD- k). *Let $\theta_0 \in \mathbb{R}^d$ be arbitrary, and $\{\alpha_j : j \in \mathbb{N}\} \subset \mathbb{R}$. SGD- k , for $k \in \mathbb{N} \cup \{\infty\}$, produces a sequence of iterates $\{\theta_j : j \in \mathbb{N}\} \subset \mathbb{R}^d$, defined by*

$$(3) \quad \theta_{j+1} = \theta_j - \frac{\alpha_{j+1}}{k} \sum_{l=j+1}^{jk+k} Q_{Z_l} \theta_j + r_{Z_l},$$

where Z_l are i.i.d. random variables such that $\mathbb{P}[Z_1 = i] = p_i$ for $i = 1, \dots, N$.

REMARK 10. *When p_i are not defined by the problem, as in [Problem 1](#), we simply require that all $p_i > 0$ and that they sum to one. In the case where p_i are defined by the problem, as in [Problem 2](#), then there is no ambiguity.*

REMARK 11. *Note, for the $k = \infty$ case, we recover gradient descent for the weighted objective function defined in [Lemma 4](#). Moreover, the sampling scheme is with replacement. While it has been observed that sampling without replacement is often superior in performance, we do not consider this further here.*

The standard analysis of any SGD method requires relating the optimality gaps between subsequent iterations. This relationship is computed in [Lemma 12](#).

LEMMA 12. *For [Problem 1](#), let $\{\theta_j : j + 1 \in \mathbb{N}\}$ be iterates generated by SGD- k . If [Assumption 8](#) holds, then $\exists \gamma \geq 0$ such that $\bar{M} := \bar{F} - (1 + \gamma)\bar{Q}^3 \succeq 0$, and for any $j + 1 \in \mathbb{N}$,*

$$(4) \quad \begin{aligned} & \mathbb{E}[(\theta_{j+1} - \beta^*)' \bar{Q}(\theta_{j+1} - \beta^*) \mid \theta_j] \\ &= (\theta_j - \beta^*)' \bar{Q}(\theta_j - \beta^*) - 2\alpha_{j+1}(\theta_j - \beta^*)' \bar{Q}^2(\theta_j - \beta^*) \\ &+ \alpha_{j+1}^2 \left(1 + \frac{\gamma}{k}\right) (\theta_j - \beta^*)' \bar{Q}^3(\theta_j - \beta^*) + \alpha_{j+1}^2 \frac{1}{k} (\theta_j - \beta^*)' \bar{M}(\theta_j - \beta^*). \end{aligned}$$

Proof. Note, by the properties of [Problem 1](#), we can rewrite the SGD- k update as $\theta_{j+1} = \theta_j - \frac{\alpha_{j+1}}{k} \tilde{Q}_j(\theta_j - \beta^*)$, where $\tilde{Q}_j = \sum_{l=j+1}^{jk+k} Q_{Z_l}$. We note that $\mathbb{E}[\tilde{Q}_j] = \sum_{l=j+1}^{jk+k} \mathbb{E}[Q_{Z_l}] = k\bar{Q}$, and $\mathbb{E}[\tilde{Q}_j \bar{Q} \tilde{Q}_j] = (k^2 - k)\bar{Q}^3 + k\bar{F}$. Moreover, when [Assumption 8](#) holds, $\mathbb{E}[\tilde{Q}_j \bar{Q} \tilde{Q}_j] = (k^2 + \gamma k)\bar{Q}^3 + k\bar{M}$. The results follow by a direct substitution and the preceding calculations. \square

Using [Lemma 12](#) and a convexity argument, we have the following bound.

REMARK 13. *In the results below, when $r = d$, we mean that $\lambda_1 \geq \dots \geq \lambda_d > 0$.*

LEMMA 14. *For [Problem 1](#), let $\{\theta_j : j + 1 \in \mathbb{N}\}$ be iterates generated by SGD- k . Let $\lambda_1 \geq \dots \geq \lambda_r > 0$ and $\lambda_{r+1} = \dots = \lambda_d = 0$ denote the eigenvalues of \bar{Q} for some $r \in \{1, \dots, d\}$. If [Assumption 8](#) holds, then $\exists \gamma \geq 0$ such that for any $j + 1 \in \mathbb{N}$,*

$$\begin{aligned} & \mathbb{E}[(\theta_{j+1} - \beta^*)' \bar{Q}(\theta_{j+1} - \beta^*)] \\ & \geq \mathbb{E}[(\theta_j - \beta^*)' \bar{Q}(\theta_j - \beta^*)] \left[1 - 2\alpha_{j+1}\lambda_m + \alpha_{j+1}^2 \left\{ \left(1 + \frac{\gamma}{k}\right) \lambda_m^2 + \frac{1}{k}s \right\} \right] \end{aligned}$$

where

1. $m = r$ if $2 \left[\left(1 + \frac{\gamma}{k}\right) (\lambda_r + \lambda_{r-1}) \right]^{-1} \leq \alpha_{j+1}$ or $\alpha_{j+1} < 0$,
2. $m = 2, \dots, r-1$ if

$$2 \left[\left(1 + \frac{\gamma}{k}\right) (\lambda_m + \lambda_{m-1}) \right]^{-1} \leq \alpha_{j+1} \leq 2 \left[\left(1 + \frac{\gamma}{k}\right) (\lambda_m + \lambda_{m+1}) \right]^{-1},$$

3. and $m = 1$ if $0 \leq \alpha_{j+1} \leq 2 \left[\left(1 + \frac{\gamma}{k}\right) (\lambda_1 + \lambda_2) \right]^{-1}$,

and

$$(5) \quad s = \min \left\{ \frac{v'(\bar{F} - (1 + \gamma)\bar{Q}^3)v}{v'\bar{Q}v} : v \in \mathbb{R}^d, v'\bar{Q}v \neq 0 \right\} \geq 0.$$

Proof. Using [Lemmas 7](#) and [12](#), on the event $(\theta_j - \beta^*)' \bar{Q}(\theta_j - \beta^*) = 0$,

$$\mathbb{E}[(\theta_{j+1} - \beta^*)' \bar{Q}(\theta_{j+1} - \beta^*) | \theta_j] \geq c(\theta_j - \beta^*)' \bar{Q}(\theta_j - \beta^*),$$

for any $c \in \mathbb{R}$. So, we now consider what happens in the case $(\theta_j - \beta^*)' \bar{Q}(\theta_j - \beta^*) \neq 0$. Let γ be as defined by [Assumption 8](#). By [Lemma 12](#) and (5),

$$\begin{aligned} \mathbb{E}[(\theta_{j+1} - \beta^*)' \bar{Q}(\theta_{j+1} - \beta^*) | \theta_j] & \geq (\theta_j - \beta^*)' \bar{Q}(\theta_j - \beta^*) \times \\ & \left[1 - 2\alpha_{j+1} \sum_{i=1}^d \lambda_i w_i + \alpha_{j+1}^2 \left(1 + \frac{\gamma}{k}\right) \sum_{i=1}^d \lambda_i^2 w_i + \alpha_{j+1}^2 \frac{1}{k}s \right], \end{aligned}$$

where, for orthonormal eigenvectors $\{u_i\}$ corresponding to eigenvalues $\{\lambda_i\}$,

$$(6) \quad w_i = \frac{\lambda_i [u_i'(\theta_j - \beta^*)]^2}{(\theta_j - \beta^*)' \bar{Q}(\theta_j - \beta^*)}.$$

Notice that $w_i \geq 0$ and $\sum_{i=1}^d w_i = 1$. Hence, we have that

$$\begin{aligned} \mathbb{E}[(\theta_{j+1} - \beta^*)' \bar{Q}(\theta_{j+1} - \beta^*) | \theta_j] & \geq (\theta_j - \beta^*)' \bar{Q}(\theta_j - \beta^*) \times \\ & \left[\sum_{i=1}^d w_i \left\{ 1 - 2\alpha_{j+1}\lambda_i + \alpha_{j+1}^2 \left(1 + \frac{\gamma}{k}\right) \lambda_i^2 \right\} + \alpha_{j+1}^2 \frac{1}{k}s \right], \end{aligned}$$

which can be lower bounded by placing all the weights, w_i , on the λ_i , $i \in \{1, \dots, r\}$, that minimizes

$$(7) \quad 1 - 2\alpha_{j+1}\lambda_i + \alpha_{j+1}^2 \left(1 + \frac{\gamma}{k}\right) \lambda_i^2.$$

When $\alpha_{j+1} < 0$, (7) is minimized when $i = r$. Now we consider the case where $\alpha_{j+1} \geq 0$. Since the eigenvalues are ordered and (7) is a quadratic function of the eigenvalue, we need only consider the relationship between adjacent pairs of eigenvalues, and, without loss of generality, we can also take all the non-zero eigenvalues to be distinct. A simple calculation shows that for $i = 1, \dots, r-1$, $\alpha_{j+1} \leq 2 \left[(1 + \frac{\gamma}{k}) (\lambda_i + \lambda_{i+1}) \right]^{-1}$, is equivalent to

$$1 - 2\alpha_{j+1}\lambda_i + \alpha_{j+1}^2 \left(1 + \frac{\gamma}{k} \right) \lambda_i^2 \leq 1 - 2\alpha_{j+1}\lambda_{i+1} + \alpha_{j+1}^2 \left(1 + \frac{\gamma}{k} \right) \lambda_{i+1}^2.$$

From this fact and combining the cases when $(\theta_j - \beta^*)' \bar{Q}(\theta_j - \beta^*)$ is zero or positive, the result follows. \square

In light of the lower bound in [Lemma 14](#), we may want to know when the multiplicative term is larger than, equal to, or less than one, which correspond to a diverging, stable, or shrinking lower bound. This result is summarized next and follows from a straightforward calculation.

LEMMA 15. *Suppose $\lambda_m > 0$.*

$$\left| 1 - 2\alpha_{j+1}\lambda_m + \alpha_{j+1}^2 \left\{ \left(1 + \frac{\gamma}{k} \right) \lambda_m^2 + \frac{1}{k}s \right\} \right| \leq 1,$$

if and only if $0 \leq \alpha_{j+1} \leq 2\lambda_m \left[\left(1 + \frac{\gamma}{k} \right) \lambda_m^2 + \frac{1}{k}s \right]^{-1}$.

We are now ready for our main result that states how the geometry of the stochastic optimization problem, the batch size k and the learning rate determine if SGD- k is repelled by a minimizer.

THEOREM 16. *For [Problem 1](#), let $\{\theta_j : j+1 \in \mathbb{N}\}$ be the iterates generated by SGD- k , and let $\lambda_1 \geq \dots \geq \lambda_r > 0$ and $\lambda_{r+1} = \dots = \lambda_d = 0$ denote the eigenvalues of \bar{Q} for some $r \in \{1, \dots, d\}$ (see [Remark 13](#)). Moreover, suppose [Assumption 8](#) holds, and let γ and s be as in [Lemma 14](#). Define*

$$\mathcal{M} = \left\{ m \in \{2, \dots, r\} : \frac{s}{\lambda_{m-1}\lambda_m} - \gamma > k \right\}, \text{ and } M = \begin{cases} \min \mathcal{M} & \mathcal{M} \neq \emptyset \\ r+1 & \mathcal{M} = \emptyset \end{cases}.$$

If either $\alpha_{j+1} < 0$, or if

$$\alpha_{j+1} > \frac{2\lambda_{M-1}}{\left(1 + \frac{\gamma}{k} \right) \lambda_{M-1}^2 + \frac{1}{k}s}$$

for any $j+1 \in \mathbb{N}$, then

$$(8) \quad \mathbb{E} [(\theta_{j+1} - \beta^*)' \bar{Q}(\theta_{j+1} - \beta^*)] > \mathbb{E} [(\theta_j - \beta^*)' \bar{Q}(\theta_j - \beta^*)].$$

Proof. If $\alpha_{j+1} < 0$ then by [Lemmas 14](#) and [15](#), the conclusion follows. Hence, we worry only about $\alpha_{j+1} > 0$. We will need the following observation. For any $m = 2, \dots, r$,

$$(9) \quad \frac{s}{\lambda_{m-1}\lambda_m} - \gamma > k \Leftrightarrow \frac{2}{\left(1 + \frac{\gamma}{k} \right) (\lambda_{m-1} + \lambda_m)} > \frac{2\lambda_m}{\left(1 + \frac{\gamma}{k} \right) \lambda_m^2 + \frac{1}{k}s}.$$

Suppose $M = r+1$, then for any $m \in \{2, \dots, r\}$ it follows that

$$\frac{2}{\left(1 + \frac{\gamma}{k} \right) (\lambda_m + \lambda_{m-1})} \leq \frac{2\lambda_m}{\left(1 + \frac{\gamma}{k} \right) \lambda_m^2 + \frac{1}{k}s}.$$

Therefore, by [Lemma 15](#), (8) holds if the hypothesis holds.

We now consider what happens when $M \in \{2, \dots, r\}$. Then for any $m \geq M$, (9) holds. By [Lemmas 14](#) and [15](#), if for any $m \geq M$,

$$\frac{2}{(1 + \frac{\gamma}{k})(\lambda_m + \lambda_{m-1})} \leq \alpha_{j+1} \leq \frac{2}{(1 + \frac{\gamma}{k})(\lambda_m + \lambda_{m+1})},$$

or, in the case when $m = r$, α_{j+1} is just greater than the lower bound, then (8) holds. To summarize, we have the following unrefined result: when $M < r + 1$, if

$$\frac{2}{(1 + \frac{\gamma}{k})(\lambda_M + \lambda_{M-1})} \leq \alpha_{j+1},$$

then (8) holds.

To refine the lower bound to recover the result, we need the following observation: for $m = 2, \dots, r$,

$$(10) \quad \frac{s}{\lambda_m \lambda_{m-1}} - \gamma \leq k \Leftrightarrow \frac{2}{(1 + \frac{\gamma}{k})(\lambda_m + \lambda_{m-1})} \leq \frac{2\lambda_{m-1}}{(1 + \frac{\gamma}{k})\lambda_{m-1}^2 + \frac{1}{k}s}.$$

Therefore, by the definition of M , for any $m \in \{2, \dots, r\}$ such that $m < M$, (10) holds. By [Lemmas 14](#) and [15](#), and the unrefined result, it follows that for $M \in \{2, \dots, r\}$, if

$$\alpha_{j+1} > \frac{2\lambda_{M-1}}{(1 + \frac{\gamma}{k})\lambda_{M-1}^2 + \frac{1}{k}s},$$

then (8) holds. \square

Before discussing the implications of [Theorem 16](#) on our motivating question (i.e., why do SB methods seem to avoid sharp minima and prefer flat minima, while LB methods seem to be agnostic?), we remark on three notable features of [Theorem 16](#). First, there is a vagueness about the choices of γ and s . Up until now, we have not specified how to choose γ and, consequently, s . The ideal choice of γ would minimize the lower bound on α_{j+1} as much as possible. While we are working on an exact mathematical treatment, we can give an intuitive understanding of what happens. Note, in general, when γ decreases, s increases. If γ is in an interval such that the value of M is fixed, then decreasing γ ends up increasing the lower bound, as we have seen from our observations. Second, if γ can be reduced such that M decreases, then we would expect the lower bound to decrease. However, in our experiments, we did not observe a situation where reducing γ resulted in a change in M .

The second notable feature about [Theorem 16](#) is methodological: it brings SGD- k for $k \in \mathbb{N}$ and Gradient Descent under a single uniform treatment. In fact, by computing the upper bound analogue to [Lemma 14](#) and using the same sequence of steps in proving [Theorem 16](#), we can find guarantees for a reduction in the optimality gap, which we state in the following theorem. Note, the proof is similar to that of [Theorem 16](#) and, consequently, is in [Appendix B](#).

THEOREM 17. *For [Problem 1](#), let $\{\theta_j : j + 1 \in \mathbb{N}\}$ be the iterates generated by SGD- k , and let $\lambda_1 \geq \dots \geq \lambda_r > 0$ and $\lambda_{r+1} = \dots = \lambda_d = 0$ denote the eigenvalues of \bar{Q} for some $r \in \{1, \dots, d\}$ (see [Remark 13](#)). Moreover, suppose [Assumption 8](#) holds. Then $\exists \gamma \geq 0$ such that*

1. *If $t/(\lambda_1 \lambda_r) - \gamma \leq k$ and $0 < \alpha_{j+1} < 2\lambda_1 \left[(1 + \frac{\gamma}{k}) \lambda_1^2 + \frac{1}{k}t \right]^{-1}$,*
2. *Or, if $k < t/(\lambda_1 \lambda_r) - \gamma$ and $0 < \alpha_{j+1} < 2\lambda_r \left[(1 + \frac{\gamma}{k}) \lambda_r^2 + \frac{1}{k}t \right]^{-1}$,*

where

$$(11) \quad t = \max \left\{ \frac{v'(\bar{F} - (1 + \gamma)\bar{Q}^3)v}{v'\bar{Q}v} : v \in \mathbb{R}^d, v'\bar{Q}v \neq 0 \right\},$$

then $\mathbb{E} [(\theta_{j+1} - \beta^*)'\bar{Q}(\theta_{j+1} - \beta^*)] < \mathbb{E} [(\theta_j - \beta^*)'\bar{Q}(\theta_j - \beta^*)]$.

REMARK 18. [Theorem 17](#) can be readily extended to a proof of convergence by specifying that α_{j+1} are fixed or decay sufficiently slowly. For a fixed learning rate, we can show that the optimality gap decays exponentially fast.

We note that we readily recover the well known necessary conditions for convergence of Gradient Descent (e.g., Eq. 1.23 in [\[1\]](#)). Moreover, by considering [Theorems 16](#) and [17](#) together, it seems that there may exist problems and choices of k and γ such that the upper bound for convergence and lower bound for divergence coincide.

The third important feature of [Theorem 16](#) and, by extension, [Theorem 17](#), is their implications for designing sampling distributions p_1, \dots, p_N such that we can achieve the fastest rates of convergence possible, which seems to continue to be a topic of interest (e.g., [\[7\]](#)). For example, we can determine optimal values of p_1, \dots, p_N , in a sense, by solving

$$\begin{aligned} & \min_{p_1, \dots, p_N, \gamma} \frac{t}{\lambda_1 \lambda_r} - \gamma \\ & \text{subject to } \bar{F} \succeq (1 + \gamma)\bar{Q}^3. \end{aligned}$$

We can also define a problem to find lower-bound optimal values of p_1, \dots, p_N . While this problem has important practical consequences, especially if the solution or an approximate solution can be trivially calculated, we will not pursue this further here.

We now interpret the implications of [Theorems 16](#) and [17](#) for answering our main question of interest: why do SB methods seem to avoid sharp minima and prefer flat minima, while LB methods seem to be agnostic? We recall that the pervading, intuitive explanation for why SB methods avoid sharp minima is that their variability allows it to escape these minima. However, [Theorems 16](#) and [17](#) suggest an alternative, deterministic mechanism for this behavior.

To begin, we will use [Theorem 16](#) to explain the deterministic reason why SB methods are more likely to escape from a sharp minimizer in comparison to LB methods. To do so, we will refer to the lower bound $2\lambda_{M-1} [(1 + \frac{\gamma}{k}) \lambda_{M-1}^2 + \frac{1}{k}s]^{-1}$ in [Theorem 16](#) as the divergence bound. We note two deterministic properties of the divergence bound: (1) as k increases, the denominator shrinks and the divergence bound increases, and (2) as k increases, M decreases and the divergence bound increases. Therefore, for intervals of k where M remains fixed, we see that as k increases, the divergence bound increases. Moreover, for intervals of k where M decreases, we see that as k increases, the divergence bound increases. Therefore, these two properties together guarantee that SB methods have access to more learning rates that guarantee that they will escape from a minimizer and LB methods have access to fewer learning rates that guarantee that they will escape from a minimizer.

We now use [Theorem 17](#) to explain the deterministic reason why SB methods and LB methods have similarly ability to converge to flat minimizers. To do so, take $\gamma = 0$ and define $\rho \geq 0$ such that $t = \rho\lambda_1\lambda_r$. Then, given the definition of t , we can loosely interpret ρ as higher-order curvature information for a minimizer. Using this

interpretation of ρ , define

$$u(k) = \begin{cases} \frac{2}{\lambda_1 + \lambda_r \rho/k} & \rho < k \\ \frac{2}{\lambda_r + \lambda_1 \rho/k} & k \leq \rho, \end{cases}$$

for $k \in \mathbb{N}$, where $u(k)$ is the upper bound on the learning rates in [Theorem 17](#) with the values of t and γ substituted with $\rho \lambda_1 \lambda_r$ and 0, respectively. Then, for very flat minima with $\rho \ll 1$, we see that $u(k) \approx 2\lambda_1^{-1}$ regardless of the choice of k . Hence, for minima with basins that are nearly planar, both SB and LB methods have access to nearly the same range learning rates that guarantee convergence.

To summarize the interpretations of [Theorems 16](#) and [17](#): in comparison to LB methods, SB methods have a larger range of learning rates that guarantee escape from sharp minima but a similar range of learning rates that guarantee convergence to flat minima.

2.2. Mathematical Characterization for the Inhomogeneous Problem.

Here, we characterize the behavior of SGD- k for [Problem 2](#) based on the batch-size, learning rate and local geometry of the equivalent objective function defined in [Lemma 6](#). Before following the standard analysis program, we will need to introduce some notation. Let β^* be as in [Lemma 6](#), and define $\epsilon_i = Q_i \beta^* + r_i$, $\bar{m} = \sum_{i=1}^N p_i Q_i \bar{Q} r_i$ and $\bar{\varphi} = \sum_{i=1}^N p_i r_i' \bar{Q} r_i$. We now state the recursion relating the optimality gap between adjacent iterates. Note, the proofs of the results below are similar to those of the preceding section and, consequently, are in [Appendix B](#).

LEMMA 19. *For [Problem 2](#), let $\{\theta_j : j + 1 \in \mathbb{N}\}$ be iterates generated by SGD- k . If [Assumption 8](#) holds, then $\exists \gamma \geq 0$ such that $\bar{M} : \bar{F} - (1 + \gamma) \bar{Q}^3 \succeq 0$, and for any $j + 1 \in \mathbb{N}$,*

$$\begin{aligned} \mathbb{E} [(\theta_{j+1} - \beta^*)' \bar{Q} (\theta_{j+1} - \beta^*) \mid \theta_j] &= (\theta_j - \beta^*)' \bar{Q} (\theta_j - \beta^*) - 2\alpha_j (\theta_j - \beta^*)' \bar{Q}^2 (\theta_j - \beta^*) \\ &+ \alpha_{j+1}^2 \left(1 + \frac{\gamma}{k}\right) (\theta_j - \beta^*)' \bar{Q}^3 (\theta_j - \beta^*) + \alpha_{j+1}^2 \frac{1}{k} (\theta_j - \beta^*)' \bar{M} (\theta_j - \beta^*) \\ &+ 2\alpha_{j+1}^2 \frac{1}{k} (\theta_j - \beta^*)' (\bar{F} \beta^* + \bar{m}) + \alpha_{j+1}^2 \frac{1}{k} (\beta^* \bar{F} \beta^* + 2\bar{m}' \beta^* + \bar{\varphi}). \end{aligned}$$

For $k = \infty$ (i.e., Gradient Descent), we see that the analysis reduces to that of [Problem 1](#). Therefore, for the remaining results, we only consider the case of $k \in \mathbb{N}$. The next lemma states an upper bound on the recursion in the preceding result.

LEMMA 20. *For [Problem 2](#), let $\{\theta_j : j + 1 \in \mathbb{N}\}$ be iterates generated by SGD- k , $k \in \mathbb{N}$. Let $\lambda_1 \geq \dots \geq \lambda_r > 0$ and $\lambda_{r+1} = \dots = \lambda_d = 0$ denote the eigenvalues of \bar{Q} for some $r \in \{1, \dots, d\}$. If [Assumption 8](#) holds, then there are $\gamma \geq 0$ and $c > 0$ such that*

$$\begin{aligned} \mathbb{E} [(\theta_{j+1} - \beta^*)' \bar{Q} (\theta_{j+1} - \beta^*)] &\leq \mathbb{E} [(\theta_j - \beta^*)' \bar{Q} (\theta_j - \beta^*)] \left[1 - 2\alpha_{j+1} \lambda_m + \alpha_{j+1}^2 \left\{ \left(1 + \frac{\gamma}{k}\right) \lambda_m^2 + \frac{t+c}{k} \right\} \right] \\ &+ \frac{\alpha_{j+1}^2}{k} \left(\beta^* \bar{F} \beta^* + 2\bar{m}' \beta^* + \bar{\varphi} + \frac{(\bar{F} \beta^* + \bar{m})' \bar{Q}^\dagger (\bar{F} \beta^* + \bar{m})}{c} \right) \end{aligned}$$

where t is defined in [Theorem 17](#) and

1. $m = r$ when $0 \leq \alpha_{j+1} \leq 2 \left[\left(1 + \frac{\gamma}{k}\right) (\lambda_1 + \lambda_r) \right]^{-1}$,
2. and $m = 1$ when $2 \left[\left(1 + \frac{\gamma}{k}\right) (\lambda_1 + \lambda_r) \right]^{-1} \leq \alpha_{j+1}$ or $\alpha_{j+1} < 0$.

Using the preceding lemma, we can state an analogue to [Theorem 17](#) for the inhomogeneous case.

THEOREM 21. *For [Problem 2](#), let $\{\theta_j : j + 1 \in \mathbb{N}\}$ be the iterates generated by SGD- k , $k \in \mathbb{N}$, and let $\lambda_1 \geq \dots \geq \lambda_r > 0$ and $\lambda_{r+1} = \dots = \lambda_d = 0$ denote the eigenvalues of \bar{Q} for some $r \in \{1, \dots, d\}$ (see [Remark 13](#)). Moreover, suppose [Assumption 8](#) holds. Then $\exists \gamma \geq 0$ and $\exists c > 0$ such that*

1. *If $(t + c + \bar{\sigma}/E_j)/(\lambda_1 \lambda_r) - \gamma \leq k < \infty$ and*

$$0 < \alpha_{j+1} < 2\lambda_1 \left[\frac{\bar{\sigma}}{kE_j} + \left(1 + \frac{\gamma}{k}\right) \lambda_1^2 + \frac{t+c}{k} \right]^{-1},$$

2. *Or, if $(t + c + \bar{\sigma}/E_j)/(\lambda_1 \lambda_r) - \gamma \geq k$ and*

$$0 < \alpha_{j+1} < 2\lambda_r \left[\frac{\bar{\sigma}}{kE_j} + \left(1 + \frac{\gamma}{k}\right) \lambda_r^2 + \frac{t+c}{k} \right]^{-1},$$

then $E_{j+1} < E_j$ where t is defined in [\(11\)](#), $E_j = \mathbb{E}[(\theta_j - \beta^*)' \bar{Q}(\theta_j - \beta^*)]$, and

$$\bar{\sigma} = \beta^{*'} \bar{F} \beta^* + 2\bar{m}' \beta^* + \bar{\varphi} + \frac{(\bar{F} \beta^* + \bar{m})' \bar{Q}^\dagger (\bar{F} \beta^* + \bar{m})}{c}.$$

If we compare [Theorems 17](#) and [21](#), we see that the inhomogeneous bound pays an extra penalty, c , to account for the inner product term in [Lemma 19](#). Moreover, in the inhomogeneous case, we see that the upper bound on the learning rate for a reduction in the optimality gap depends on the size of the optimality gap: as the optimality gap decreases, the learning rate must decrease at the same order. Similarly, in the inhomogeneous case, we see that the bifurcation point on k also depends on the optimality gap: as the optimality gap decreases, the learning rates will eventually be required to satisfy the bound depending on the smallest positive eigenvalue, λ_r . Hence, as the optimality gap converges to zero, α_{j+1} must be approximately less than $2k\lambda_r E_j/\bar{\sigma}$.

To see that similar results for the lower bound hold, we will compute the lower bound analogue of [Lemma 20](#) for a limited geometric case.

LEMMA 22. *For [Problem 2](#), let $\{\theta_j : j + 1 \in \mathbb{N}\}$ be iterates generated by SGD- k , $k \in \mathbb{N}$. Let $\lambda_1 \geq \dots \geq \lambda_r > 0$ and $\lambda_{r+1} = \dots = \lambda_d = 0$ denote the eigenvalues of \bar{Q} for some $r \in \{1, \dots, d\}$. If [Assumption 8](#) holds and $\gamma\lambda_m^2 + s - \bar{z} > 0$ then for any $\rho_1, \rho_2 \in (0, 1]$*

$$\begin{aligned} & \mathbb{E}[(\theta_{j+1} - \beta^*)' \bar{Q}(\theta_{j+1} - \beta^*) \mid \theta_j] \\ & \geq \rho_1 (\theta_j - \beta^*)' \bar{Q}(\theta_j - \beta^*) \left[1 - 2\alpha_{j+1} \lambda_m + \alpha_{j+1}^2 \left\{ \left(1 + \frac{\gamma}{k}\right) \lambda_m^2 + \frac{s - \bar{z}}{k} \right\} \right] \\ & + \alpha_{j+1}^2 \frac{1}{k} \rho_2 (\beta^{*'} \bar{F} \beta^* + 2\bar{m}' \beta^* + \bar{\varphi}) \times \\ & \left(1 - \frac{\frac{\alpha_{j+1}^2}{k} \bar{z}}{(1 - \rho_1) \left[1 - 2\alpha_{j+1} \lambda_m + \alpha_{j+1}^2 \left\{ \left(1 + \frac{\gamma}{k}\right) \lambda_m^2 + \frac{s}{k} \right\} \right] + \rho_1 \frac{\alpha_{j+1}^2}{k} \bar{z}} \right), \end{aligned}$$

where s is defined in [\(5\)](#); m is as in [Lemma 14](#); and $\bar{z} = \frac{(\bar{F} \beta^* + \bar{m})' \bar{Q}^\dagger (\bar{F} \beta^* + \bar{m})}{\beta^{*'} \bar{F} \beta^* + 2\bar{m}' \beta^* + \bar{\varphi}}$.

Note, when $\rho_1 = 1$, [Lemma 22](#) reduces to [Lemma 14](#) with an additional penalty of \bar{z} . Then, taking $\rho_1 = 1$, an exact analogue of [Theorem 16](#) will hold for the inhomogeneous case. If we consider what happens when $\rho_1 \in (0, 1)$ we will see that m will be determined by s, \bar{z} , the optimality gap and k in a form similar to [Theorem 21](#); however, we will not state this case as the algebra is complex and offers no additional information in light of [Theorems 16](#) and [21](#). In summary, the results for the inhomogeneous case are sufficiently similar to the results for the homogeneous case and, for our purposes, it is sufficient to use the homogeneous results with the understanding that without a diminishing step-size we will not have convergence to a minimizer for the inhomogeneous case but we will have stability about the minimizer in some sense.

Now, with the the results of this section, we consider the behavior of SGD- k on more general problems. Although the results of [Theorems 16](#) and [17](#) can be extended with some modifications to smooth convex problems and certain cases of non-smooth convex problems under additional assumptions, this is wholly uninteresting for nonconvex problems. A rigorous theoretical treatment of the nonconvex problem is nontrivial, and, for now, we explore the extension of [Theorems 16](#) and [17](#) to the nonconvex case using numerical studies.

3. Numerical Studies on a Homogeneous Non-convex Problem. We explore a nonconvex, two-dimensional problem with a sufficiently rich and modifiable surface whose components have homogeneous minima that will allow us to probe how well [Theorems 16](#) and [17](#) generalize to nonconvex stochastic optimization problems. In [subsection 3.1](#), we describe the function and provide several examples of its surface for different parameters. In [subsection 3.2](#), we study several instances of the test function and study how well the conclusions of [Theorems 16](#) and [17](#) extend to this problem.

3.1. The Quadratic-Circle Function. First, we describe the quadratic-circle function and discuss how its parameters modify the properties of the function. The quadratic-circle function is the minimum of two functions: a quadratic basin function and a circular basin function. The quadratic type function is defined as

$$(12) \quad g(x) = q_1(x_2 - q_2 x_1^2 - q_3)^2.$$

The quadratic type function, g , traces out a parabola in the plane of its arguments where $g(x)$ is zero and increases quadratically as x_2 deviates from this parabola. The parameters q_1 and q_2 are non-negative. The parameter q_1 determines how quickly $g(x)$ increases off of the parabola (i.e., its sharpness), and the remaining parameters determine the shape of the parabola. Examples of the quadratic basin function are shown in [Figure 10](#).

The circular basin function is a piece-wise function defined as

$$(13) \quad h(x) = \begin{cases} c_4 & \|x\| \leq c_2 \\ c_4 + c_1 & \|x\| \geq c_3 \\ c_4 + c_1 \left(\frac{\|x\| - c_2}{c_3 - c_2} \right)^3 \left[6 \left(\frac{\|x\| - c_2}{c_3 - c_2} \right)^2 - 15 \left(\frac{\|x\| - c_2}{c_3 - c_2} \right) + 10 \right] & \text{otherwise} \end{cases},$$

where all of the parameters are non-negative. The circular basin function, h , defines a flat region encompassed by a circle of radius c_2 and defines a flat region outside of a circle of radius c_3 . Between these two circles and for $c_2 > 0$, we have a twice differentiable function which ensures that $h(x)$ is twice continuously differentiable. When the ratio between c_3 and c_2 decreases, the steepness of the basin's walls increases

(i.e., the walls are sharper). Increasing the distance between c_4 and c_1 has a similar outcome. Examples of the circular basin function are shown in [Figure 11](#).

The quadratic-circle function is then defined to be the minimum of the quadratic basin function and the circular basin function:

$$(14) \quad f(x) = \min\{h(x), g(x)\}.$$

Examples of the quadratic-circle function are shown in [Figure 12](#).

REMARK 23. *The quadratic-circle function has curves of non-differentiability. If an iterate is at a point of non-differentiability, the gradient will always be selected to be the quadratic component. However, any point randomly selected from the plane using a measure which admits a probability density function with respect to the Lebesgue measure has a probability of zero of ever hitting a non-differentiable point.*

The nonconvex objective function that we will use is a summation of N functions of the form (14) with different parameters for the quadratic and circular components. For later reference, we define this objective function presently.

PROBLEM 24 (Quadratic-Circular Sums). *Let g_1, \dots, g_N be functions as specified (12) and h_1, \dots, h_N be functions as specified by (13). The quadratic-circular sums objective function is*

$$(15) \quad \sum_{i=1}^N p_i \min\{g_i(x), h_i(x)\},$$

where p_i are positive valued and sum to one. The quadratic-circular sums problem is to minimize this objective function in $(-10, 10) \times (-20, 15) \subset \mathbb{R}^2$.

3.2. SGD-k on the Quadratic-Circular Sums Objective. In general, we will design four model quadratic-circular sums problems to analyze. All of the model functions have two minimizers in the region of interest: one for the circular-basic component at $(0, 0)$ and one for quadratic basin component at $(0, -15)$. However, the sharpness of the basins about the minima distinguish the four model functions. The first model, Model 1, is characterized by having at least one large eigenvalue about each minimum. The second model, Model 2, is characterized by having at least one large eigenvalue for the circular basin minimizer and only small eigenvalues for the quadratic basin minimizer. Model 3 is characterized by having at least one large eigenvalue for the quadratic basin minimum and only small eigenvalues for the circular basin minimum. Model 4 is characterized by having only small eigenvalues for both minima. Note, the size of these eigenvalues are relative to the other models and not some general baseline. For clarity, each of the four model quadratic-circular sums objective functions are visualized and described further in [Figure 13](#).

Now, in order to understand how [Theorems 16](#) and [17](#) extend to these four model problems, we will need to estimate the geometric parameters γ , s and t , the lower bound on the learning rate for divergence and the upper bound on the learning rate for convergence as defined in the results. Because the minima are not exactly quadratics, we will estimate the geometric parameters by averaging over quadratic approximations to points within a small neighborhood of the minimizer and then compute the lower bounds for divergence and upper bounds for convergence from these geometric parameter estimates. The lower bound estimates are reported in [Table 1](#). Note, for the lower bounds, k_{\max} is the largest integer smaller than $\frac{s}{\lambda_{r-1}\lambda_r} - \gamma$. The upper

TABLE 1

Estimated lower bound values for divergence for the two minimizers of the Quadratic-Circular Sums objective functions for the four different parameters sets.

	Circ. Minimum				Quad. Minimum	
	$k = 1$	$k = 0.99k_{\max}$	$k = 2.0k_{\max}$	$k = \infty$	$k = 1$	$k = \infty$
Model 1	$3.560e + 11$	$3.583e + 11$	$3.583e + 11$	$3.583e + 11$	$4.977e + 00$	$4.981e + 00$
Model 2	$3.339e + 11$	$3.360e + 11$	$3.360e + 11$	$3.360e + 11$	$9.954e + 02$	$9.961e + 02$
Model 3	$1.266e + 15$	$1.273e + 15$	$1.273e + 15$	$1.273e + 15$	$4.977e + 00$	$4.981e + 00$
Model 4	$1.269e + 15$	$1.277e + 15$	$1.277e + 15$	$1.277e + 15$	$9.954e + 02$	$9.961e + 02$

TABLE 2

Estimated upper bound values for convergence for the two minimizers of the Quadratic-Circular Sums objective functions for the four different parameters sets.

	Circ. Minimum				Quad. Minimum	
	$k = 1$	$k = 0.99k_{\max}$	$k = 2.0k_{\max}$	$k = \infty$	$k = 1$	$k = \infty$
Model 1	$8.318e - 05$	$1.541e + 11$	$2.013e + 11$	$2.874e + 11$	$4.977e + 00$	$4.981e + 00$
Model 2	$8.456e - 05$	$1.624e + 11$	$2.157e + 11$	$3.180e + 11$	$9.954e + 02$	$9.961e + 02$
Model 3	$5.655e - 06$	$6.222e + 14$	$8.282e + 14$	$1.226e + 15$	$4.977e + 00$	$4.981e + 00$
Model 4	$5.511e - 06$	$6.267e + 14$	$8.264e + 14$	$1.201e + 15$	$9.954e + 02$	$9.961e + 02$

bounds are reported in Table 2. Note, for the upper bounds, k_{\max} is the the integer closest to $\frac{t}{\lambda_r \lambda_1} - \gamma$.

There are several notable features in Tables 1 and 2, but since the main points are transferable between these two cases, we focus on the lower bound results. First, the flatter minima tend to have a larger lower bound for divergence. For example, since the circular-basin minima in Models 3 and 4 are flatter than the circular-basin minima in Models 1 and 2, the lower bound for divergence is nearly ten thousand fold larger. Similarly, since the quadratic minima in Models 2 and 4 are flatter than the quadratic basin minima in Models 1 and 3, the lower bound for divergence is over a hundred times larger. Second, for the circular basin minimum, there is a very minor difference between the lower bounds for divergence between the $k = 1$ and $k = \infty$ cases. This is to be expected since the circular symmetry of the basin implies that its condition number is one and since the value of $\gamma \ll 1$ for this circular minimizer.

Guided by the quantities in Tables 1 and 2, we now run SGD-1 and SGD- ∞ (i.e. Gradient Descent) on the four models with different learning rates and starting points, and analyze the properties of these iterates in order to determine how well Theorems 16 and 17 generalize to the quadratic-circular sums objective function.

Experimental Procedure. We study four experimental factors: the model, the learning method, the initialization point, and the learning rate. The model factor has four levels as given by the four model objective functions shown in Figure 13. The learning method has two levels which are SGD-1 or GD. The initialization point also has two levels: either the initialization point is selected randomly with a uniform probability from a disc of radius 10^{-8} centered about the circular basin minimizer, or the initialization point is selected randomly with a uniform probability from a disc of radius 10^{-8} centered about the quadratic basin minimizer. The learning rate has levels that are conditional on the initialization point. If the initialization point is near the minimizer of the circular basin, then the learning rate takes on values $10^{10}, 5(10^{10}), 10^{11}, 5(10^{11}), 10^{12}, 5(10^{12})$. If the initialization point is near the minimizer of the circular basin, then the learning rate takes on values 1, 4, 16, 64, 256, 1024.

For each unique collection of the levels of the four factors, one hundred independent runs are executed with at most twenty iterations. For each run, the euclidean distance between the iterates and the circular basin minimizer and the euclidean dis-

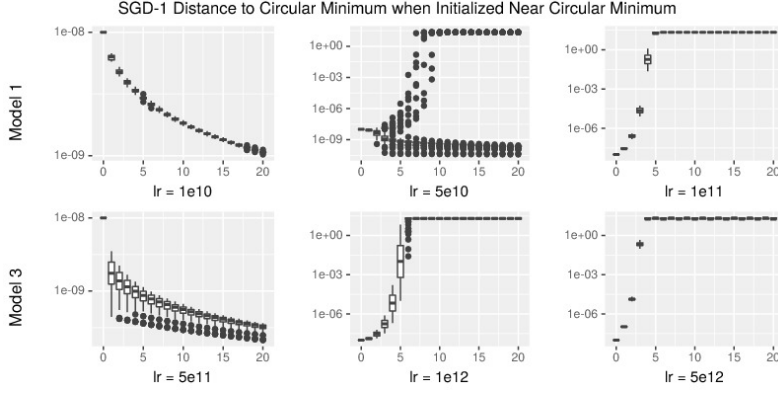


FIG. 1. The behavior of SGD-1 on Models 1 and 3 when initialized near the circular minimum. The y-axis shows the distance (in logarithmic scale) between the iterates and the circular minimum for all runs of the specified model and the specified learning rate.

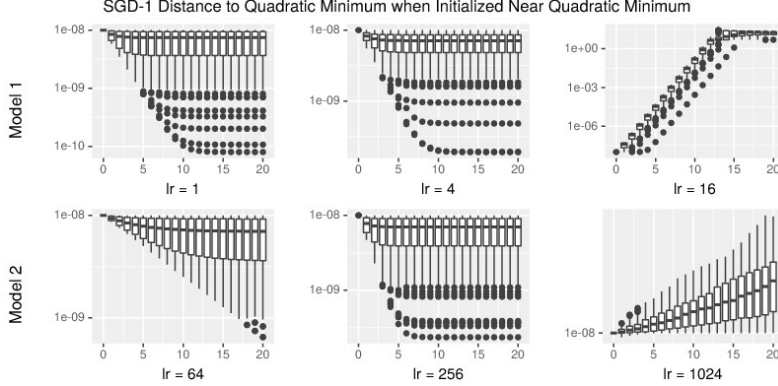


FIG. 2. The behavior of SGD-1 on Models 1 and 2 when initialized near the quadratic minimum. The y-axis shows the distance (in logarithmic scale) between the iterates and the quadratic minimum for all runs of the specified model and the specified learning rate.

tance between the iterates and the quadratic basin minimizer are recorded.

Results and Discussion. Note, we will primarily focus on the divergence perspective because the convergence perspective offers an almost identical discussion. Also note that the results of SGD- k on Models 1 and 2 and Models 3 and 4 are similar when initialized around the circular basin minimizer, and the results of SGD- k on Models 1 and 3 and Models 2 and 4 are similar when initialized around the quadratic basin minimizer. Hence, when we discuss the circular basin minimizer, we will compare Models 1 and 3, but we could have just as easily replaced Model 1 with Model 2 or Model 3 with Model 4 and the discussion would be identical. Similarly, when we discuss the quadratic basin minimizer, we will compare Models 1 and 2, but we could have replaced the results of Model 1 with Model 3 or Model 2 with Model 4 and the discussion would be identical. We now describe several observations and discuss how well [Theorem 16](#) anticipates these experimental observations. At the end, we discuss how variability falls short of explaining these experimental observations.

[Figure 1](#) shows the distance between the iterates and the circular basin minimizer

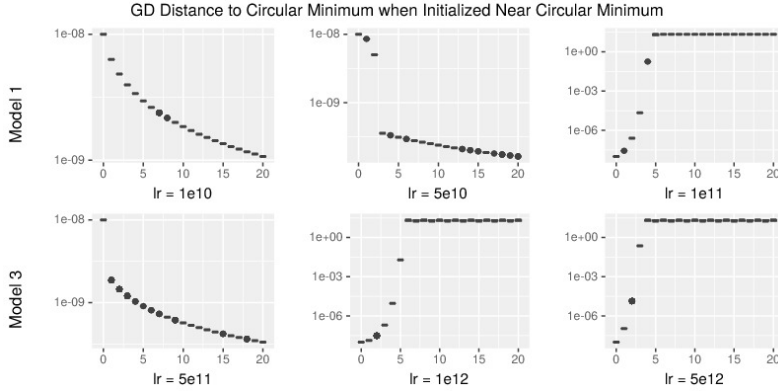


FIG. 3. The behavior of GD on Models 1 and 3 when initialized near the circular minimum. The y-axis shows the distance (in logarithmic scale) between the iterates and the circular minimum for all runs of the specified model and the specified learning rate.

for the one hundred independent runs of SGD-1 for the specified model and the specified learning rate when initialized near the circular basin minimizer. The learning rates that are displayed are the ones where a transition in the convergence-divergence behavior of the method occur for the specific model. Specifically, SGD-1 begins to diverge for learning rates between 5×10^{10} and 10^{11} for Model 1 and between 5×10^{11} and 10^{12} for Model 3. Similarly, Figure 2 shows the distance between the iterates and the quadratic basin minimizer for the one hundred independent runs of SGD-1 for the specified model and the specified learning rate when initialized near the quadratic basin minimizer. SGD-1 begins to diverge for learning rates between 4 and 16 for Model 1 and between 256 and 1024 for Model 2. In light of Theorem 16, this behavior is expected: according to Theorem 16, relatively flatter minima will have larger lower bounds for divergence on learning rates in comparison to sharper minima. More importantly, we see that the estimates in Table 1 are conservative, but produce estimates on the lower bounds that are informative, especially in the case of the quadratic basin.

Figure 3 shows the distance between the iterates and the circular basin minimizer for the one hundred independent runs of GD for the specified model and the specified learning rate when initialized near the circular basin minimizer. If we compare Figures 1 and 3, we notice that, for Model 1 and learning rate 5×10^{10} , the runs of GD converge whereas some of the runs for SGD-1 diverge. Although we do not report the results for all of the models or all of the learning rates, we note the boundary for divergence-convergence for GD are smaller than those of SGD-1. In light of Theorem 16, this behavior is expected: according to Theorem 16, as the batch-size, k , increases, the lower bound on the learning rates for divergence increases. Therefore, we should expect that at those boundary learning rates where some SGD-1 runs are stable and others diverge, for GD, we should only see stable runs, and, indeed, this is what the comparison of Figures 1 and 3 shows.

Figure 4 shows the distance between the iterates and the circular basin minimizer for the one hundred independent runs of SGD-1 and the one hundred independent runs of GD for the specified method and the specified learning rate when initialized near the quadratic basin minimizer. In Figure 4, we see that for the learning rates that lead to divergence from the quadratic basin minimizer (compare to the top three subplots of

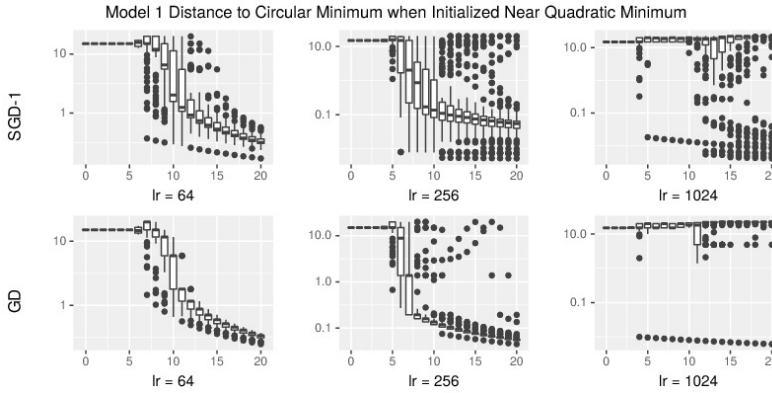


FIG. 4. The behavior of SGD-1 and GD on Model 1 when initialized near the quadratic minimum for select learning rates. The y-axis shows the distance (in logarithmic scale) between the iterates and the circular minimum for all runs of the specified method and the specified learning rate.

Figure 1) are in some cases able to converge to the circular minimizer. Again, in light of Theorem 16, this is expected: according to Theorem 16, the learning rates shown in Figure 4 guarantee divergence from the quadratic minimizer and are sufficiently small that they can lead to convergence to the circular minimizer. However, we notice in Figure 4 that as the learning rate increases, even though the learning rate is below the divergence bound for the circular minimizer, the iterates for SGD-1 and GD are diverging from both the circular and quadratic minima and are converging to the corners of the feasible region.

Here, it does appear that variability plays a role in determining if SGD-1 and GD will converge to the circular minimizer or to the corners of the feasible region. However, it seems that as the learning rate increases, it is more likely for the iterates of both SGD-1 and GD to converge to the corners of the feasible region. This suggests that there is some systematic (i.e., non-random) reason why the corners of the feasible region are being preferred to the circular basin. As describing this systematic property is not within the scope of our current work, we will not describe it further, but we will use it simply to state the variability alone is not sufficient to describe why this behavior occurs.

Moreover, suppose variability is the reason why a method is able to escape from a sharp minimizer. Well, most obviously, this does not explain why we are able to find learning rates that cause GD, a deterministic method, to escape from a minimizer with arbitrary geometric properties. Second, if variability is the reason why a method is able to escape from a sharp minimizer, then we might expect some runs of SGD-1 to diverge from a minimizer for a few iterations and then, by its inherent randomness, converge to the same minimizer. However, we fail to see such behavior in Figures 1 and 2. In fact, we see the opposite: once a sequence of iterates begins to diverge from a minimizer, they continue to do so in almost a predictable manner.

To summarize, we see that variability falls short of explaining the convergence-divergence behavior of SGD- k , yet Theorems 16 and 17 do quite well at explaining the convergence and divergence properties of SGD- k , and, more importantly, are able to provide numerical estimates to show when convergence or divergence occur. In order to further elaborate our results, we now consider a less trivial nonconvex optimization problem which has multiple minima, a more complex surface, and is much higher

dimensional.

4. Numerical Studies on an Inhomogeneous Non-convex Problem. We now explore the modification of Styblinski-Tang (ST) function [9], which was originally introduced in the neural network literature and served as a test function owing to its complex surface yet simple mathematical form. The d -dimensional ST function is given by

$$(16) \quad f(x) = \frac{1}{2} \sum_{i=1}^d c_{i,1} x_i^4 + c_{i,2} x_i^2 + c_{i,3} x_i,$$

where $c_{i,1}, c_{i,3}$ are non-negative scalars, and $c_{i,2}$ is a non-positive scalar. Using this equation we can define the following problem, for which two dimensional examples are plotted in [Figure 14](#).

PROBLEM 25 (Styblinski-Tang Sums). *Let f_1, \dots, f_N be functions as specified by (16) of some dimension d . The Styblinski-Tang sums objective function is*

$$(17) \quad \sum_{i=1}^N p_i f_i(x),$$

where p_i are positive valued and sum to one. The Styblinski-Tang sums problem is to minimize the objective function in $(-5, 5)^d \subset \mathbb{R}^d$.

While the analysis of [Problem 25](#) may seem superfluous given the analysis of [Problem 24](#), it is a fundamentally different problem because the component functions of [Problem 25](#) do not have a common minimizer; that is, [Problem 25](#) is the nonconvex analogue of [Problem 2](#). Therefore, the results of [subsection 2.2](#) are more applicable in this context. However, as we mentioned in [subsection 2.2](#), if we switch from studying convergence and divergence of SGD- k to studying the stability and divergence of SGD- k around minima, then, because of the structural similarities of the results in [subsection 2.1](#) and the results in [subsection 2.2](#), using the simpler estimates on the lower bounds for divergence and the upper bounds for convergence as provided by [Theorems 16](#) and [17](#) will be sufficient in our numerical studies.

To study the stability and divergence properties of SGD- k on [Problem 25](#), we consider three randomly generated realizations of [Problem 25](#) which we label Model 1, Model 2, and Model 3. Model 1 is of dimension ten, has 2^{10} minima, and has $N = 200$ components; Model 2 is of dimension fifty, has 2^{50} minima, and has $N = 1000$ components; Model 3 is of dimension one hundred, has 2^{100} minima, and has $N = 2000$ components.

For each model, the flattest and sharpest minima are identified. For each minimizer, the threshold values of $\frac{t}{\lambda_1 \lambda_r} - \gamma$ are reported in [Table 3](#). Using these threshold values, estimates for the upper bounds on convergence and lower bounds on divergence for the learning rates, according to [Theorems 16](#) and [17](#), are reported in [Tables 4](#) and [5](#) (note, the definition of k_{\max} is the same as in [Tables 1](#) and [2](#) respectively). In general, the flatter minima have a higher tolerance with respect to divergence and convergence for larger learning rates in comparison to the sharp minima. However, this relationship is not guaranteed as we see in [Table 5](#) for Model 3. Here, we see that the sharpest minimizer has a slightly higher for larger learning rates. This is due to the t term in the bounds, indicating that it cannot be neglected. We now look at how well our estimates based on our theory compare to numerical experiments of SGD- k for different values of k on the three models.

TABLE 3
Transition points for sharpest and flattest minima of different ST sums problems.

Minimizer	Model 1	Model 2	Model 3
Flat	$5.096e + 00$	$1.343e + 02$	$3.920e + 02$
Sharp	$3.260e + 00$	$1.186e + 02$	$2.668e + 02$

TABLE 4
Estimated lower bound values for divergence for the sharpest and flattest minima of different ST sums problems.

k	Model 1		Model 2		Model 3	
	Flat	Sharp	Flat	Sharp	Flat	Sharp
1.0	$9.001e - 03$	$7.682e - 03$	$2.134e - 02$	$1.951e - 02$	$2.598e - 02$	$1.871e - 02$
100.0	$9.814e - 02$	$8.133e - 02$	$6.831e - 01$	$6.117e - 01$	$1.221e + 00$	$8.561e - 01$
200.0	$1.033e - 01$	$8.546e - 02$	$8.100e - 01$	$7.225e - 01$	$1.590e + 00$	$1.106e + 00$
350.0	$1.057e - 01$	$8.737e - 02$	$8.800e - 01$	$7.833e - 01$	$1.827e + 00$	$1.264e + 00$
500.0	$1.067e - 01$	$8.815e - 02$	$9.116e - 01$	$8.106e - 01$	$1.942e + 00$	$1.341e + 00$
∞	$1.091e - 01$	$9.004e - 02$	$9.947e - 01$	$8.823e - 01$	$2.279e + 00$	$1.563e + 00$

Experimental Procedure. We study four experimental factors: the model, the batch size, the initialization point, and the learning rate. The model factor has three levels that correspond to the three models described above. The batch size will take the values corresponding to SGD-1, SGD-200, SGD-500, and Gradient Descent. The initialization point will be randomly selected from a uniform distribution on a ball whose radius will take values $\{10^{-3}, 10^{-2}, 10^{-1}, 1\}$ and is centered at either the sharpest minimizer or the flattest minimizer. The learning rates will be linear combinations of the upper and lower bounds. Specifically, if u is the upper bound in [Theorem 17](#) and l is the lower bound in [Theorem 16](#), then the learning rates will be $1.5l$, 0.5 , $0.5(u + l)$, or $0.5u$.

For each unique collection of the levels of the four factors, one hundred independent runs are executed with at most twenty iterations. For each run, the euclidean distances between the iterates and the minimizer near the initialization point are recorded.

Results and Discussion. We now summarize our experimental results, discuss how [Theorems 16](#) and [17](#) explain the important aspects of our experimental results, and discuss how variability alone fails to describe the aforementioned features. Note, the results Models 1, 2 and 3 are nearly identical for the purposes of our discussion, and so we will feature Model 1 only in our discussion below. However, we generate the same figures for Model 2 and 3 for comparison in [Appendix E](#).

[Figure 5](#) shows the distance between SGD- k iterates and the flat minimizer on Model 1 for different batch sizes and different learning rates when SGD- k is initialized near the flat minimizer. We note that, regardless of batch size, the iterates are diverging from the flat minimizer and are converging to the corners of the feasible region for learning rates $1.5l$ and $0.5(u + l)$. On the other hand, for the learning rate $0.5u$, we see stability for $k = 1, 200, 500$ about the minimizer and we see convergence for GD (i.e., $k = \infty$). Similarly, [Figure 6](#) shows the distance between SGD- k iterates and the sharp minimizer on Model 1 for different batch sizes and different learning rates when SGD- k is initialized near the sharp minimizer. We note that, regardless of batch size, the iterates are diverging from the sharp minimizer and converging to the corners of the feasible region for learning rates $1.5l$ and $0.5(u + l)$. On the other hand, for the learning rate $0.5u$, we see stability for $k = 1, 200, 500$ about the sharp minimizer and we see convergence for GD (i.e., $k = \infty$).

Taking the results in [Figures 5](#) and [6](#) together, we see that we are able to use

TABLE 5

Estimated upper bound values for convergence for the sharpest and flattest minima of different ST sums problems.

k	Model 1		Model 2		Model 3	
	Flat	Sharp	Flat	Sharp	Flat	Sharp
1.0	$2.319e - 03$	$2.250e - 03$	$8.603e - 04$	$8.334e - 04$	$7.587e - 04$	$9.089e - 04$
100.0	$4.268e - 02$	$3.781e - 02$	$7.925e - 02$	$7.621e - 02$	$7.345e - 02$	$8.594e - 02$
200.0	$4.632e - 02$	$4.087e - 02$	$1.174e - 01$	$1.049e - 01$	$1.423e - 01$	$1.629e - 01$
350.0	$4.808e - 02$	$4.234e - 02$	$1.329e - 01$	$1.180e - 01$	$2.379e - 01$	$2.303e - 01$
500.0	$4.882e - 02$	$4.296e - 02$	$1.403e - 01$	$1.243e - 01$	$2.812e - 01$	$2.539e - 01$
∞	$5.064e - 02$	$4.447e - 02$	$1.613e - 01$	$1.418e - 01$	$3.742e - 01$	$3.337e - 01$

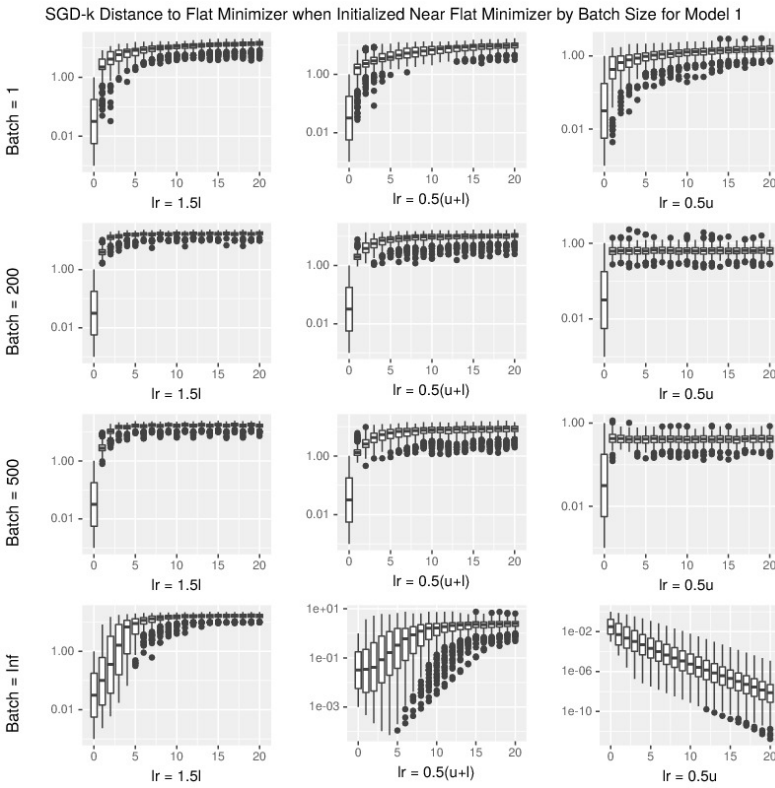


FIG. 5. The behavior of SGD- k on Model 1 for different batch sizes when initialized near the flat minimizer. The y-axis shows the distance (in logarithmic scale) between the iterates and the flat minimizer for all runs of the specified batch size and specified learning rate.

Theorems 16 and 17 to find learning rates that either ensure divergence from or stability about a minimizer if we know its local geometric properties. Again, if we suppose that variability does play a role here, we might suspect that some of the runs might remain stable for the flat minimizer when Theorem 16 predicts divergence or that some runs might diverge for the sharp minimizer when Theorem 17 predicts stability, especially when $k = 1$. However, we see that all runs behave uniformly and either diverge or remain stable according to the predictions of Theorems 16 and 17. Thus, we see that variability does not seem to play a role with regards to divergence from or stability about minima regardless of the batch size.

For a different perspective, Figure 7 shows the distance between SGD- k iterates

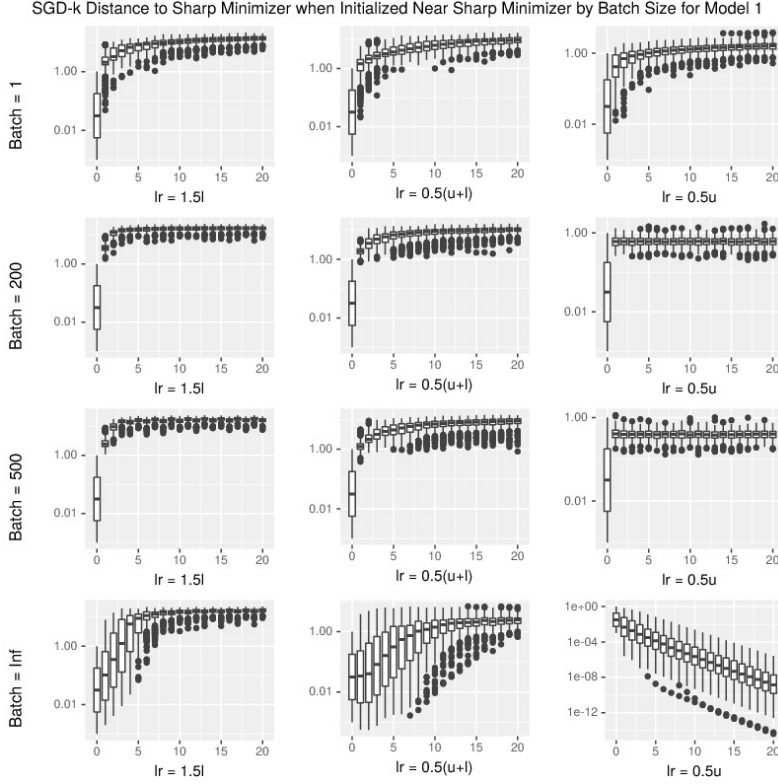


FIG. 6. The behavior of SGD- k on Model 1 for different batch sizes when initialized near the sharp minimizer. The y-axis shows the distance (in logarithmic scale) between the iterates and the sharp minimizer for all runs of the specified batch size and specified learning rate.

and the flat minimizer on Model 1 for different starting radii and different learning rates when SGD- k is initialized near the flat minimizer. We note that, regardless of the starting radius, the iterate are diverging from the flat minimizer and are converging to the corners of the feasible region for learning rates $1.5l$ and $0.5(u + l)$. On the other hand, for the learning rate $0.5u$, we see stability and even convergence for all of the runs regardless of the starting radius. Similarly, Figure 8 shows the distance between SGD- k iterates and the sharp minimizer on Model for different starting radii and different learning rates when SGD- k is initialized near the sharp minimizer. We note that, regardless of the starting radius, the iterates are diverging from the sharp minimizer and are converging to the corners of the feasible region for learning rates $1.5l$ and $0.5(u + l)$. On the other hand, for learning rate $0.5u$, we see stability about and even convergence to the sharp minimizer.

Taking the results in Figures 7 and 8 together, we see that we are able to use Theorems 16 and 17 to find learning rates that either ensure divergence from or stability about a minimizer if we know its local geometric properties. Again, if we suppose that variability does play a role here, we might suspect that some of the runs might remain stable, especially with a start radius of 0.001, for the flat minimizer when Theorem 16 predicts divergence, or that some runs might diverge for the sharp minimizer, especially with a start radius of 1.0, when Theorem 17 predicts stability. However, we see that all runs behave uniformly and either diverge or remain stable

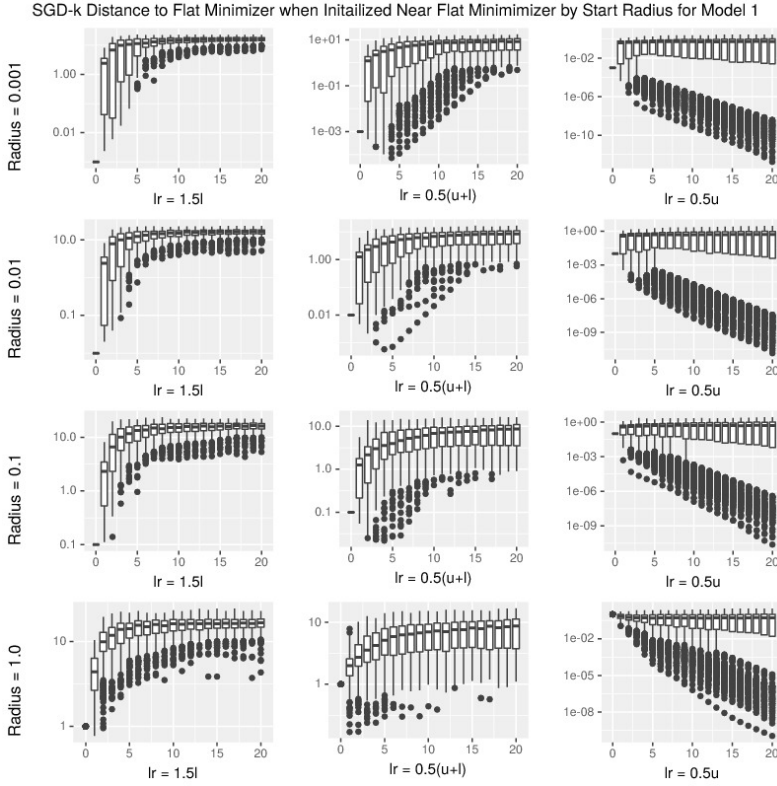


FIG. 7. The behavior of SGD- k on Model 1 for different starting radii when initialized near the flat minimizer. The y-axis shows the distance (in logarithmic scale) between the iterates and the flat minimizer for all runs of the specified starting radius and specified learning rate.

according to the predictions of Theorems 16 and 17. Thus, we see that variability does not seem to play a role with regards to divergence from or stability about the minima regardless of the starting radius.

To summarize, we see that Theorems 16 and 17 are able to explain the stability and divergence behavior of SGD- k even for the nonconvex inhomogeneous problem. Moreover, we are able to use Theorems 16 and 17 to give a quantitative explanation of when stability will occur or when divergence will occur. On the other hand, using variation alone to explain these properties falls short of even qualitatively explaining our numerical observations.

5. Conclusion. In this work, we offer a deterministic mechanism to explain why small-batch SGD- k methods are able to escape from sharp minima and converge to flat minima and to explain why large-batch SGD- k methods (including Gradient Descent) seem to be unable to escape from sharp minima. Specifically, we state that given a batch size and the expected local geometry of a minimizer there are precise lower bounds on the learning rate that guarantee that SGD- k will diverge from the minimizer and there are precise upper bounds on the learning rate that guarantee that SGD- k will converge to or remain stable about the minimizer. We then used numerical experiments to show that our precise statements about the lower and upper bounds are able to translate to homogeneous and inhomogeneous nonconvex optimization

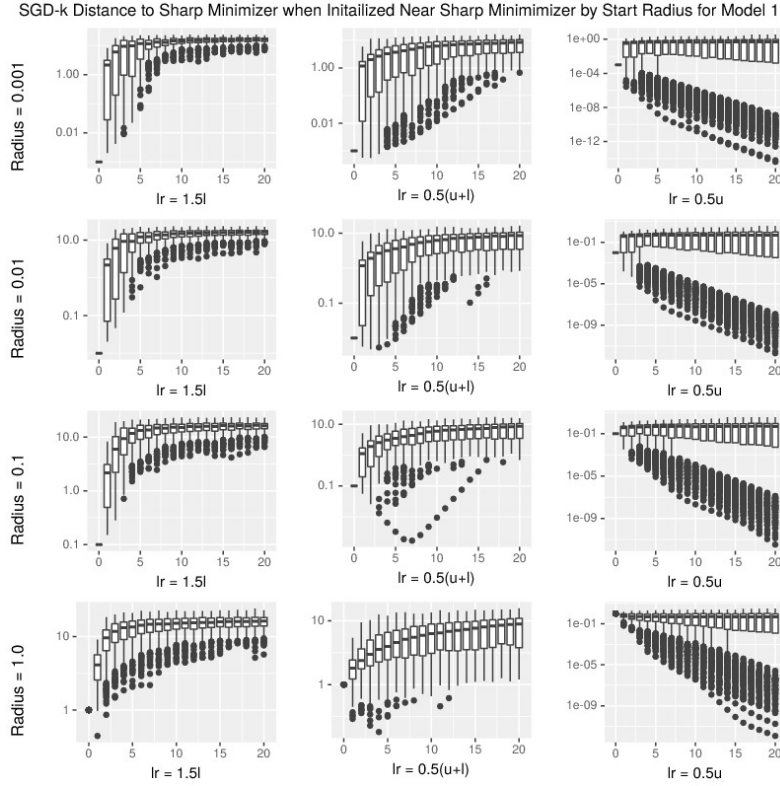


FIG. 8. The behavior of SGD- k on Model 1 for different starting radii when initialized near the sharp minimizer. The y-axis shows the distance (in logarithmic scale) between the iterates and the sharp minimizer for all runs of the specified starting radius and specified learning rate.

problems.

We will conclude with a general lesson for how to choose batch sizes and learning rates so that specific minima can be selected. First, if we desire to converge to a flat minimizer, which is often the case in machine learning problems, it is best to use small batch sizes and to start with very large learning rates and to slowly decrease them so that sharp minima can be systematically avoided. However, we note that it is important to constrain the feasible region as choosing very large learning rates may force the iterates far away from the minima and result in numerical overflow problems. Second, if we desire to converge to a sharp minimizer, there is no way for selecting for this minimizer using a non-adaptive learning rate. The only hope is to use a large batch size and to use small learning rates, although this can introduce other challenges in the inhomogeneous case [8].

Acknowledgments. We would like to acknowledge Mihai Anitescu for his guidance throughout the research process and for his financial support.

REFERENCES

- [1] D. P. BERTSEKAS, *Nonlinear programming*, Athena scientific Belmont, 1999.
- [2] R. COLLOBERT AND J. WESTON, *A unified architecture for natural language processing: Deep neural networks with multitask learning*, in Proceedings of the 25th international conference

on Machine learning, ACM, 2008, pp. 160–167.

- [3] G. HINTON, L. DENG, D. YU, G. E. DAHL, A.-R. MOHAMED, N. JAITLY, A. SENIOR, V. VANHOUCKE, P. NGUYEN, T. N. SAINATH, ET AL., *Deep neural networks for acoustic modeling in speech recognition: The shared views of four research groups*, IEEE Signal Processing Magazine, 29 (2012), pp. 82–97.
- [4] N. S. KESKAR, D. MUDIGERE, J. NOCEDAL, M. SMELYANSKIY, AND P. T. P. TANG, *On large-batch training for deep learning: Generalization gap and sharp minima*, 2017.
- [5] A. KRIZHEVSKY, I. SUTSKEVER, AND G. E. HINTON, *Imagenet classification with deep convolutional neural networks*, in Advances in neural information processing systems, 2012, pp. 1097–1105.
- [6] F. MEZZADRI, *How to generate random matrices from the classical compact groups*, arXiv preprint math-ph/0609050, (2006).
- [7] D. NEEDELL, R. WARD, AND N. SREBRO, *Stochastic gradient descent, weighted sampling, and the randomized kaczmarz algorithm*, in Advances in Neural Information Processing Systems, 2014, pp. 1017–1025.
- [8] A. NEMIROVSKI, A. JUDITSKY, G. LAN, AND A. SHAPIRO, *Robust stochastic approximation approach to stochastic programming*, SIAM Journal on optimization, 19 (2009), pp. 1574–1609.
- [9] M. STYBLINSKI AND T.-S. TANG, *Experiments in nonconvex optimization: stochastic approximation with function smoothing and simulated annealing*, Neural Networks, 3 (1990), pp. 467–483.

Appendix A. Numerical Evidence Supporting the Moment Assumption. Our goal here is to provide numerical evidence supporting [Assumption 8](#). We will begin by detailing our experimental procedure. Then, we present summaries of our results, and discuss their implications for validating [Assumption 8](#).

Experimental Procedure. To overview, we will generate N symmetric, positive semi-definite matrices in $\mathbb{R}^{d \times d}$, randomly generate the probabilities p_1, \dots, p_N such that they sum to one, compute \bar{Q} and \bar{F} , and then compute the smallest eigenvalue of $\bar{F} - \bar{Q}^3$. If this smallest eigenvalue is non-negative, then we know that [Assumption 8](#) holds with γ at least zero for this collection of $\{p_i, Q_i\}$. We now describe each step in detail.

We generate each Q by setting $Q = U\Lambda U'$ where U is an orthonormal matrix and Λ is a diagonal, positive semi-definite matrix. The matrix U is generated by uniformly sampling from the set of all orthonormal matrices in $\mathbb{R}^{d \times d}$ [6]. The diagonal matrix Λ is specified by a lower bound $B < d$ on the number of zero eigenvalues, and the remaining non-zero eigenvalues are sampled independently and uniformly from the interval $[0, 50]$. The upper bound was selected arbitrarily. Each Q is generated independently. The lower bound B on the number of zero eigenvalues is fixed over all Q .

The probabilities p_1, \dots, p_N are selected by first drawing weights w_1, \dots, w_n independently, and uniformly over $[0, 1]$, and then dividing the weights by the sum of all the weights.

We then compute \bar{Q} and \bar{F} . However, because of some numerical imprecisions, the values of \bar{Q} and \bar{F} may not be symmetric. Therefore, we symmetrize these matrices by computing their singular value decomposition, and multiplying the singular value matrix from the left by the left singular vector matrix and from the right by the transpose of the left singular vector matrix. The maximum absolute element-wise error is recorded between the symmetrization and the original matrices computed according to their definitions.

Using the symmetrized values of \bar{F} and \bar{Q} , we then compute the eigenvalues of $\bar{F} - \bar{Q}^3$. We record the minimum value of the real components of the eigenvalues, and record the norm of the imaginary component.

We fix $d = 200$, vary N from 50 to 400 by increments of 50, and vary B from 0 to 180 by increments of 20. For each (B, N) pair, we repeat the experiment twenty times

independently, resulting in 1,600 runs. For each run, we record, as described above, the smallest real component of the eigenvalues of the difference $\bar{F} - \bar{Q}^3$, the norm of the imaginary component of the eigenvalues of the difference, the symmetrization error of \bar{Q} , and the symmetrization error of \bar{F} .

Results and Discussion. Figure 9 summarizes the smallest eigenvalue and symmetrization errors for each pair (B, N) with the full data set in the appendix. We note that none of the real components are negative, and the largest norm of the imaginary component was 0.0 over all of the runs. Given the sampling procedures for Q_i and p_i , we are uniformly sampling over the space of matrices \bar{F} and \bar{Q} for which each Q_i has eigenvalues bounded by 50. Therefore, since all of the smallest real components of the eigenvalues of the difference $\bar{F} - \bar{Q}^3$ were positive, we have reason to believe that Assumption 8 holds quite generally. While these numerical simulations do not substitute for a proof, we hope that for our current purposes, they are sufficient in quelling any doubts about the generality of Assumption 8.

Appendix B. Proofs.

Proof of Theorem 17. Suppose $(\theta_j - \beta^*)' \bar{Q}(\theta_j - \beta^*) = 0$. Then, by Lemma 7, $(\theta_j - \beta^*)' \bar{M}(\theta_j - \beta^*) = 0$. So, by Lemma 12,

$$\mathbb{E} [(\theta_{j+1} - \beta^*)' \bar{Q}(\theta_{j+1} - \beta^*) | \theta_j] \leq c(\theta_j - \beta^*)' \bar{Q}(\theta_j - \beta^*),$$

for any $c \in \mathbb{R}$. We now consider the case when $(\theta_j - \beta^*)' \bar{Q}(\theta_j - \beta^*) \neq 0$. Let γ be defined by Assumption 8. By Lemma 12 and (11),

$$\begin{aligned} \mathbb{E} [(\theta_{j+1} - \beta^*)' \bar{Q}(\theta_{j+1} - \beta^*) | \theta_j] &\leq (\theta_j - \beta^*)' \bar{Q}(\theta_j - \beta^*) \times \\ &\left[1 - 2\alpha_{j+1} \sum_{i=1}^d \lambda_i w_i + \alpha_{j+1}^2 \left(1 + \frac{\gamma}{k} \right) \sum_{i=1}^d \lambda_i^2 w_i + \alpha_{j+1}^2 \frac{1}{k} t \right], \end{aligned}$$

where w_i is defined as in (6). We can upper bound the convex sum following the same strategy as in Lemma 14; that is, we want to place all the weights, w_i , on the λ_i , $i \in \{1, \dots, r\}$ that maximizes (7). Since (7) is quadratic in λ , when $\alpha_{j+1} < 0$ or $2 \left[(1 + \frac{\gamma}{k}) (\lambda_1 + \lambda_r) \right]^{-1} \leq \alpha_{j+1}$, then (7) is maximized by λ_1 . Otherwise, (7) is maximized by λ_r . Therefore,

$$(18) \quad \begin{aligned} \mathbb{E} [(\theta_{j+1} - \beta^*)' \bar{Q}(\theta_{j+1} - \beta^*) | \theta_j] &\leq (\theta_j - \beta^*)' \bar{Q}(\theta_j - \beta^*) \times \\ &\left[1 - 2\alpha_{j+1} \lambda_m + \alpha_{j+1}^2 \left\{ \left(1 + \frac{\gamma}{k} \right) \lambda_m^2 + \frac{1}{k} t \right\} \right], \end{aligned}$$

where $m = 1$ for $\alpha_{j+1} < 0$ or $2 \left[(1 + \frac{\gamma}{k}) (\lambda_1 + \lambda_r) \right]^{-1} \leq \alpha_{j+1}$ and $m = r$ otherwise. Using Lemma 15 and proceeding as in Theorem 16, the result follows. \square

Proof of Lemma 19. Note, we will rewrite the SGD- k update as

$$\theta_{j+1} = \theta_j - \frac{\alpha_{j+1}}{k} \tilde{Q}_j(\theta_j - \beta^*) - \frac{\alpha_{j+1}}{k} \tilde{\epsilon}_j,$$

where $\tilde{Q}_j = \sum_{l=j+1}^{jk+k} Q_{Z_l}$ and $\tilde{\epsilon}_j = \sum_{l=j+1}^{jk+k} \epsilon_{Z_l}$. We also make note of the following calculations: $\mathbb{E} [\tilde{Q}_j] = \sum_{l=1}^k \mathbb{E} [Q_{Z_l}] = k\bar{Q}$, $\mathbb{E} [\tilde{\epsilon}_j] = \sum_{l=1}^k \mathbb{E} [\epsilon_l] = 0$, $\mathbb{E} [\tilde{Q}_j \bar{Q} \tilde{Q}_j] = (k^2 - k)\bar{Q}^3 + k\bar{F}$, $\mathbb{E} [\tilde{Q}_j \bar{Q} \tilde{\epsilon}_j] = k\bar{F}\beta^* + k\bar{m}$, and $\mathbb{E} [\tilde{\epsilon}_j \bar{Q} \tilde{\epsilon}_j] = k(\beta^{*\prime} \bar{F} \beta^* + 2\bar{m}' \beta^* + \bar{\varphi})$. The result follows from a direct computation, and use of the above calculations. \square

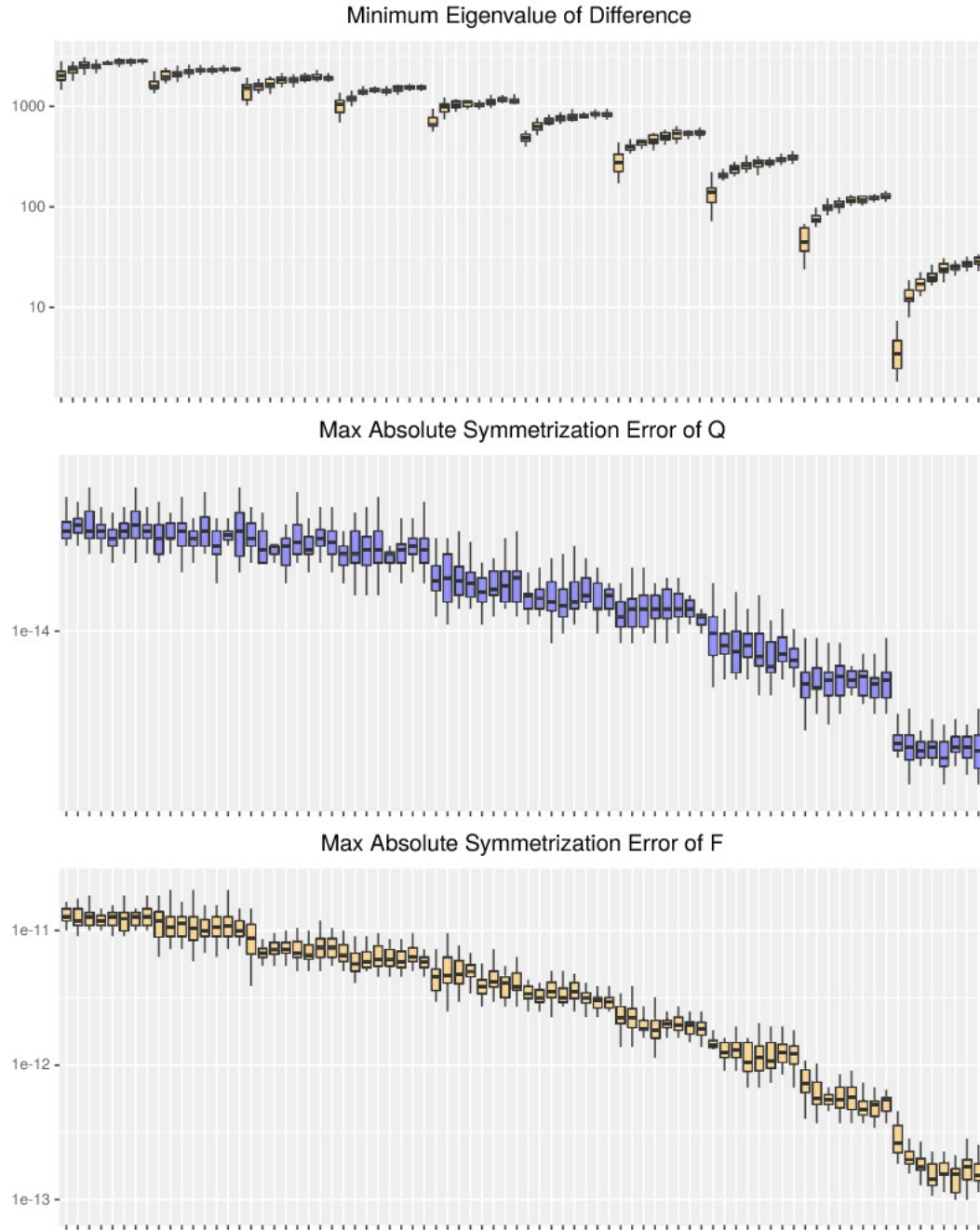


FIG. 9. Boxplots for the smallest real component of the eigenvalues of the difference $\bar{F} - \bar{Q}^3$, the symmetrization error of \bar{Q} , and the symmetrization error \bar{F} by the eighty pairs (B, N) . From left to right, the (B, N) pairs are ordered as $(0, 50), (0, 100), \dots, (0, 400), (20, 50), (20, 100), \dots, (180, 350), (180, 400)$.

Proof of Lemma 20. We can handle the case when $(\theta_j - \beta^*)' \bar{Q}(\theta_j - \beta^*) = 0$ just as we do in [Theorem 17](#). Therefore, we consider the case when $(\theta_j - \beta^*)' \bar{Q}(\theta_j - \beta^*) > 0$. Note,

$$1 - 2\alpha_{j+1}\lambda_r + \alpha_{j+1}^2 \left[\lambda_r^2 \left(1 + \frac{\gamma}{k} \right) + \frac{1}{k}t \right] \leq 1 - 2\alpha_{j+1}\lambda_1 + \alpha_{j+1}^2 \left[\lambda_1^2 \left(1 + \frac{\gamma}{k} \right) + \frac{1}{k}t \right]$$

if and only if $2\alpha_{j+1} \leq \alpha_{j+1}^2(\lambda_1 + \lambda_r) \left(1 + \frac{\gamma}{k} \right)$. Therefore, either when $\alpha_{j+1} < 0$ or when $2 \left[\left(1 + \frac{\gamma}{k} \right) (\lambda_1 + \lambda_r) \right]^{-1} \leq \alpha_{j+1}$, this inequality holds.

Using this inequality and the convex approximation method from [Lemma 14](#), we have that

$$\begin{aligned} & \mathbb{E} [(\theta_{j+1} - \beta^*)' \bar{Q}(\theta_{j+1} - \beta^*) | \theta_j] \\ & \leq (\theta_j - \beta^*)' \bar{Q}(\theta_j - \beta^*) \left[1 - 2\alpha_{j+1}\lambda_m + \alpha_{j+1}^2 \left\{ \left(1 + \frac{\gamma}{k} \right) \lambda_m^2 + \frac{1}{k}t \right\} \right] \\ & + 2\alpha_{j+1}^2 \frac{1}{k} (\theta_j - \beta^*)' (\bar{F}\beta^* + \bar{m}) + \alpha_{j+1}^2 \frac{1}{k} (\beta^* \bar{F}\beta^* + 2\bar{m}'\beta^* + \bar{\varphi}), \end{aligned}$$

where t is defined in [Theorem 17](#) and

1. $m = r$ when $0 \leq \alpha_{j+1} \leq 2 \left[\left(1 + \frac{\gamma}{k} \right) (\lambda_1 + \lambda_r) \right]^{-1}$,
2. and $m = 1$ when $2 \left[\left(1 + \frac{\gamma}{k} \right) (\lambda_1 + \lambda_r) \right]^{-1} \leq \alpha_{j+1}$ or $\alpha_{j+1} < 0$.

Since $\bar{m} = \sum_{i=1}^N p_i Q_i \bar{Q} r_i$ and $\bar{F}\beta^* = \sum_{i=1}^N p_i Q_i \bar{Q} (Q_i \beta^*)$, we can apply [Lemma 28](#) to get that

$$\begin{aligned} (\theta_j - \beta^*)' (\bar{F}\beta^* + \bar{m}) &= (\theta_j - \beta^*)' \bar{Q} \bar{Q}^\dagger (\bar{F}\beta^* + \bar{m}) \\ &\leq \left\| \bar{Q}^{1/2} (\theta_j - \beta^*) \right\|_2 \left\| \bar{Q}^{1/2} \bar{Q}^\dagger (\bar{F}\beta^* + \bar{m}) \right\|_2. \end{aligned}$$

Applying [Lemma 27](#) gives the result. \square

Proof of Theorem 21. Using [Lemma 20](#), for the appropriate m , we want to show that

$$E_{j+1} \leq E_j \left[1 - 2\alpha_{j+1}\lambda_m + \alpha_{j+1}^2 \left\{ \left(1 + \frac{\gamma}{k} \right) \lambda_m^2 + \frac{t+c}{k} \right\} \right] + \alpha_{j+1}^2 \frac{1}{k} \bar{\sigma} < E_j.$$

We see that when $\alpha_{j+1} \leq 0$ that this is not possible. Therefore, we consider when $\alpha_{j+1} > 0$. Then, rearranging the right inequality, we see that this holds when $0 < \alpha_{j+1} < 2\lambda_m \left[\left(1 + \frac{\gamma}{k} \right) \lambda_m^2 + \frac{t+c+\bar{\sigma}/E_k}{k} \right]^{-1}$.

Now, when $(t+c+\bar{\sigma}/E_j)/(\lambda_1 \lambda_r) - \gamma \leq k$ then

$$\frac{2}{\left(1 + \frac{\gamma}{k} \right) (\lambda_1 + \lambda_r)} \leq \frac{2\lambda_1}{\left(1 + \frac{\gamma}{k} \right) \lambda_1^2 + \frac{t+c+\bar{\sigma}/E_k}{k}} \leq \frac{2\lambda_r}{\left(1 + \frac{\gamma}{k} \right) \lambda_r^2 + \frac{t+c+\bar{\sigma}/E_k}{k}},$$

and when $(t+c+\bar{\sigma}/E_j)/(\lambda_1 \lambda_r) - \gamma \geq k$ then

$$\frac{2}{\left(1 + \frac{\gamma}{k} \right) (\lambda_1 + \lambda_r)} \geq \frac{2\lambda_1}{\left(1 + \frac{\gamma}{k} \right) \lambda_1^2 + \frac{t+c+\bar{\sigma}/E_k}{k}} \geq \frac{2\lambda_r}{\left(1 + \frac{\gamma}{k} \right) \lambda_r^2 + \frac{t+c+\bar{\sigma}/E_k}{k}}.$$

Hence, by [Lemma 20](#), when $m = 1$ or $m = r$, if $(t+c+\bar{\sigma}/E_j)/(\lambda_1 \lambda_r) - \gamma \leq k$ and $0 < \alpha_{j+1} < 2\lambda_1 \left[\left(1 + \frac{\gamma}{k} \right) \lambda_1^2 + \frac{t+c+\bar{\sigma}/E_k}{k} \right]^{-1}$ then $E_{j+1} < E_j$. Similarly, when $m = r$,

if $(t + c + \bar{\sigma}/E_j)/(\lambda_1 \lambda_r) - \gamma \geq k$ and $0 < \alpha_{j+1} < 2\lambda_r \left[(1 + \frac{\gamma}{k}) \lambda_r^2 + \frac{t+c+\bar{\sigma}/E_k}{k} \right]^{-1}$ then $E_{j+1} < E_j$. However, when $m = 1$, if $(t + c + \bar{\sigma}/E_j)/(\lambda_1 \lambda_r) - \gamma \geq k$ then there is no value allowable value of α_{j+1} that guarantees $E_{j+1} < E_j$. \square

Proof of Lemma 22. Using Lemmas 14 and 19, for an appropriate choice of m ,

$$\begin{aligned} & \mathbb{E} [(\theta_{j+1} - \beta^*)' \bar{Q}(\theta_{j+1} - \beta^*) \mid \theta_j] \\ & \geq (\theta_j - \beta^*)' \bar{Q}(\theta_j - \beta^*) \left[1 - 2\alpha_{j+1}\lambda_m + \alpha_{j+1}^2 \left\{ \left(1 + \frac{\gamma}{k}\right) \lambda_m^2 + \frac{1}{k}s \right\} \right] \\ & \quad + 2\alpha_{j+1}^2 \frac{1}{k} (\theta_j - \beta^*)' (\bar{F}\beta^* + \bar{m}) + \alpha_{j+1}^2 \frac{1}{k} (\beta^{*'} \bar{F}\beta^* + 2\bar{m}'\beta^* + \bar{\varphi}). \end{aligned}$$

Moreover, since $\bar{m} = \sum_{i=1}^N p_i Q_i \bar{Q} r_i$ and $\bar{F}\beta^* = \sum_{i=1}^N p_i Q_i \bar{Q}(Q_i \beta^*)$, we can apply Lemma 28 to get that

$$\begin{aligned} (\theta_j - \beta^*)' (\bar{F}\beta^* + \bar{m}) &= (\theta_j - \beta^*)' \bar{Q} \bar{Q}^\dagger (\bar{F}\beta^* + \bar{m}) \\ &\leq \left\| \bar{Q}^{1/2} (\theta_j - \beta^*) \right\|_2 \left\| \bar{Q}^{1/2} \bar{Q}^\dagger (\bar{F}\beta^* + \bar{m}) \right\|_2. \end{aligned}$$

Putting these two inequalities together, we have that

$$\begin{aligned} & \mathbb{E} [(\theta_{j+1} - \beta^*)' \bar{Q}(\theta_{j+1} - \beta^*) \mid \theta_j] \\ & \geq (\theta_j - \beta^*)' \bar{Q}(\theta_j - \beta^*) \left[1 - 2\alpha_{j+1}\lambda_m + \alpha_{j+1}^2 \left\{ \left(1 + \frac{\gamma}{k}\right) \lambda_m^2 + \frac{1}{k}s \right\} \right] \\ & \quad - 2\alpha_{j+1}^2 \frac{1}{k} \left\| \bar{Q}^{1/2} (\theta_j - \beta^*) \right\|_2 \left\| \bar{Q}^{1/2} \bar{Q}^\dagger (\bar{F}\beta^* + \bar{m}) \right\|_2 \\ & \quad + \alpha_{j+1}^2 \frac{1}{k} (\beta^{*'} \bar{F}\beta^* + 2\bar{m}'\beta^* + \bar{\varphi}). \end{aligned}$$

The result follows by applying Lemma 26, but, in order to do so, we need that

$$(19) \quad 1 - 2\alpha_{j+1}\lambda_m + \alpha_{j+1}^2 \left\{ \left(1 + \frac{\gamma}{k}\right) \lambda_m^2 + \frac{1}{k}s \right\} > \frac{\alpha_{j+1}^2}{k} \bar{z},$$

which holds under the hypotheses. \square

Appendix C. Technical Lemmas.

LEMMA 26. Suppose $x \geq 0$, $c_1, c_2, c_3 > 0$ such that $c_1 c_3 > c_2^2$. Then $\forall \rho, \sigma \in (0, 1]$,

$$c_1 x^2 - 2c_2 x + c_3 \geq \rho(c_1 - c_2^2/c_3)x^2 + \sigma c_3 \left(1 - \frac{c_2^2/c_3}{(1-\rho)c_1 + \rho c_2^2/c_3} \right) \geq 0.$$

Proof. Note if $c_1 c_3 > c_2^2$ then $c_1 - c_2^2/c_3 > 0$ and, for any $\rho \in (0, 1)$,

$$1 - \frac{c_2^2/c_3}{(1-\rho)c_1 + \rho c_2^2/c_3} = \frac{(1-\rho)(c_1 - c_2^2/c_3)}{(1-\rho)c_1 + \rho c_2^2/c_3} > 0,$$

and is equal to 0 when $\rho = 1$. Therefore, the last inequality of the statement holds.

Now, letting $\delta = (1-\rho)c_1 + \rho c_2^2/c_3$, note, for any $\rho, \sigma \in (0, 1]$,

$$\begin{aligned} & \delta \left(x - \frac{c_2}{\delta} \right)^2 + c_3 - \frac{c_2^2}{\delta} \geq \sigma \left(c_3 - \frac{c_2^2}{\delta} \right) \\ & \delta x^2 - 2c_2 x + c_3 \geq \sigma \left(c_3 - \frac{c_2^2}{\delta} \right) \\ & c_1 x^2 - 2c_2 x + c_3 \geq \rho(c_1 - c_2^2/c_3)x^2 + \sigma c_3 \left(1 - \frac{c_2^2/c_3}{(1-\rho)c_1 + \rho c_2^2/c_3} \right). \quad \square \end{aligned}$$

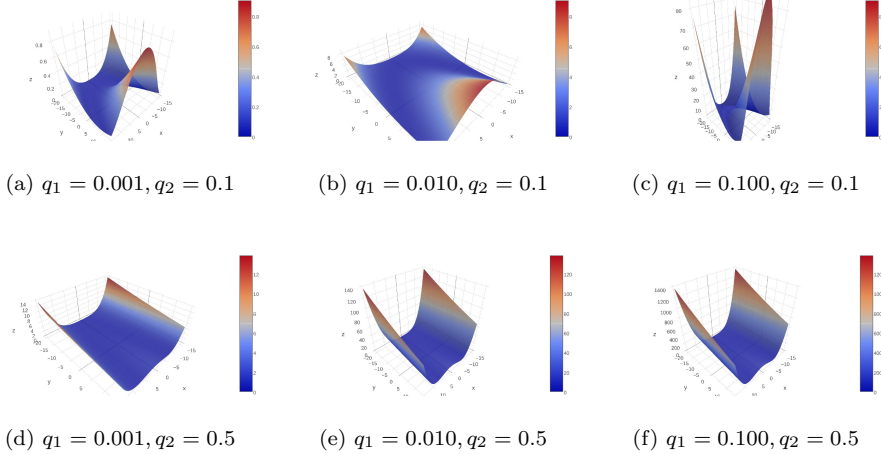


FIG. 10. Different realizations of the quadratic basin function for varying values of q_1 and q_2 , and a fixed value of $q_3 = -15.0$. Notice that as q_1 is increased, the minimizing quadratic basin has much sharper walls.

By a simpler calculation, the following statement holds.

LEMMA 27. Let $c_1 > 0$ and $c_2 > 0$. Then, for all $x \in \mathbb{R}$, $2c_2x \leq c_1x^2 + \frac{c_2^2}{c_1}$.

LEMMA 28. Suppose Q_1, \dots, Q_N are symmetric, positive semi-definite matrices. Let p_1, \dots, p_N be positive scalars. Let $\bar{Q} = \sum_{i=1}^N p_i Q_i$. Then,

$$\text{row}(\bar{Q}) \supseteq \bigcup_{i=1}^N \text{col}(Q_i \bar{Q}).$$

Moreover, for any vectors s_1, \dots, s_N , $\sum_{i=1}^N p_i Q_i \bar{Q} s_i = \bar{Q} \bar{Q}^\dagger \sum_{i=1}^N p_i Q_i \bar{Q} s_i$.

Proof. For any $\bar{Q}v = 0$, $v \bar{Q}v = 0$. Hence, $v Q_i v = 0$ for $i = 1, \dots, N$. So v is in the null space of Q_i . Therefore, the null space of \bar{Q} is contained in the null space of Q_i for each i . Hence,

$$\text{row}(\bar{Q}) = \text{null}(\bar{Q})^\perp \supseteq \bigcup_{i=1}^N \text{null}(Q_i)^\perp = \bigcup_{i=1}^N \text{col}(Q_i) \supseteq \bigcup_{i=1}^N \text{col}(Q_i \bar{Q})$$

Now, for any s_1, \dots, s_N , $\sum_{i=1}^N p_i Q_i \bar{Q} s_i \in \text{row}(\bar{Q})$. Since for any $x \in \text{row}(\bar{Q})$, $x = \bar{Q} \bar{Q}^\dagger x$, the last statement holds. \square

Appendix D. Quadratic-Circle Problem. Figures 10 to 12 contain examples of the quadratic-basin function, circular-basin function and quadratic-circle function for different parameters. Figure 13 contains visualizations of the models used in the numerical experiments.

Appendix E. Styblinski-Tang Problem.

Figure 14 shows a two-dimensional example of Problem 25.

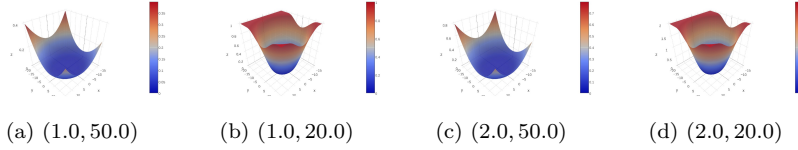


FIG. 11. Different realizations of the circular basin function for varying values of (c_1, c_3) , and fixed values of $c_2 = 5.0$ and $c_4 = 0.0$. Notice that as c_1 is increased and c_3 is decreased, the walls of the basin become much steeper.

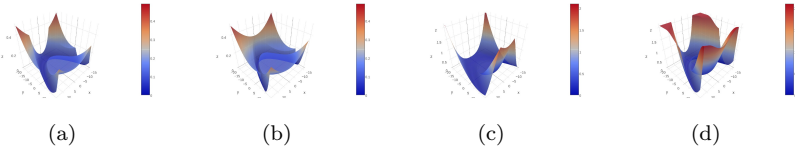


FIG. 12. Different realizations of the quadratic-circle function for different parameters of the circular basin and the quadratic basin functions.

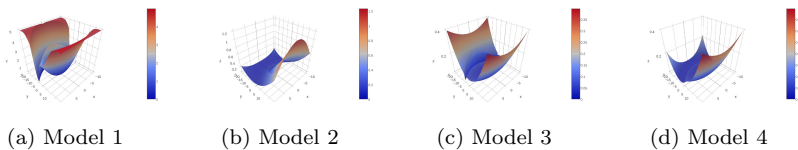


FIG. 13. The different model quadratic-circular sums objective functions. Each objective function is made up of $N = 50$ quadratic-circular functions with differing, randomly determined parameters with a specified mean parameter with the exception that c_4 and q_3 are identical for all components within a model. Also, Models 1 and 2 and Models 3 and 4 have identical mean parameter values for the circular component, while Models 1 and 3 and Models 2 and 4 have identical mean parameter values for the quadratic component.

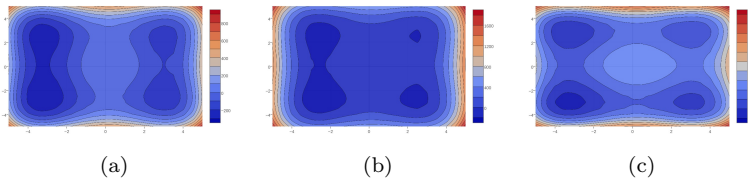


FIG. 14. Contour plots of three randomly generated ST sums objective functions in two dimensions. Notice the differing widths, depths and connectivities of the minima in these three examples; clearly, ST sums functions are able to generate a rich and diverse non-convex surface.

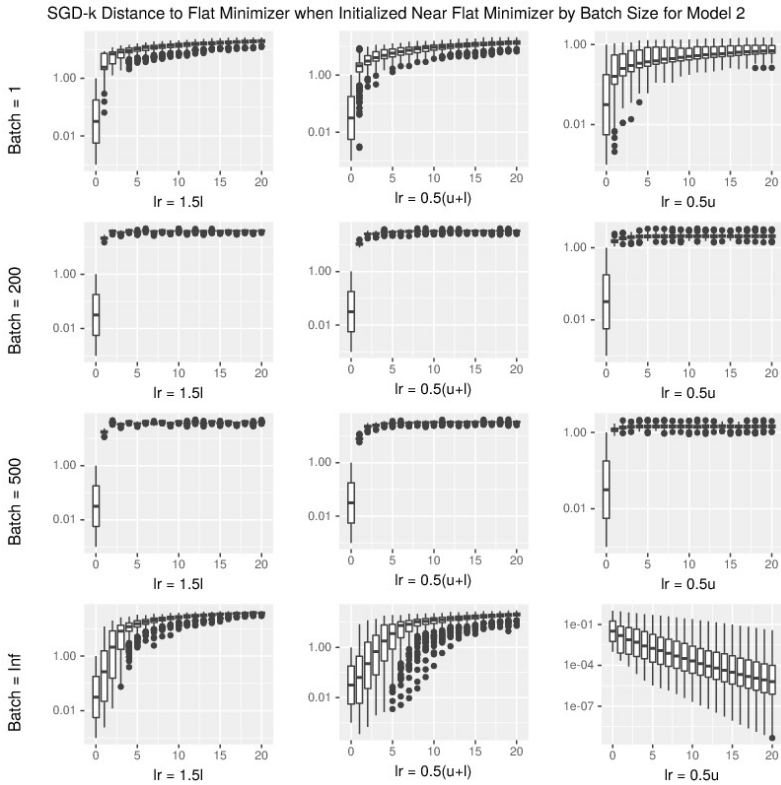


FIG. 15. The behavior of SGD-k on Model 2 for different batch sizes when initialized near the flat minimizer. The y-axis shows the distance (in logarithmic scale) between the iterates and the flat minimizer for all runs of the specified batch size and specified learning rate.

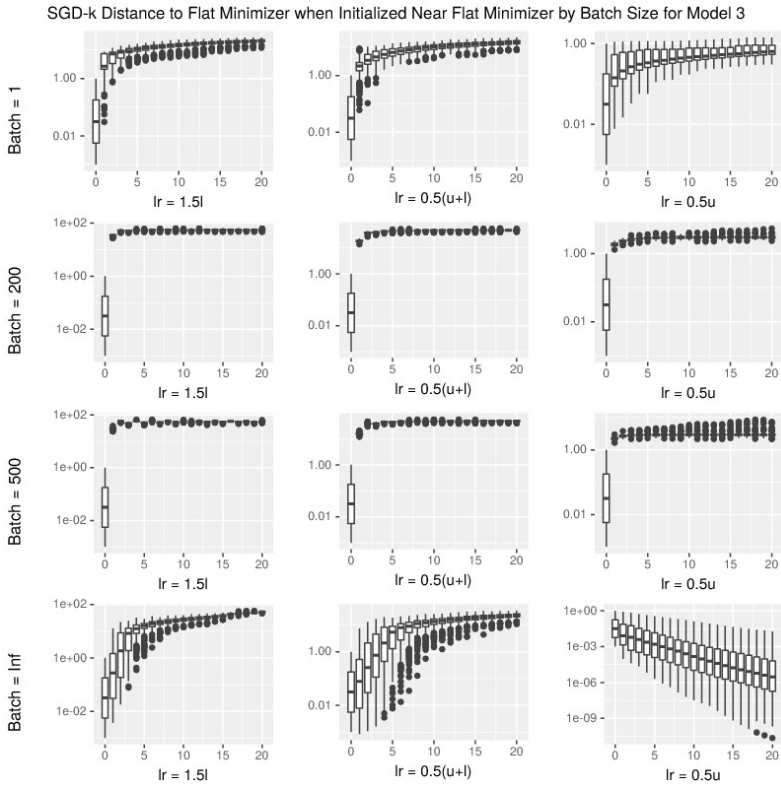


FIG. 16. The behavior of SGD-k on Model 3 for different batch sizes when initialized near the flat minimizer. The y-axis shows the distance (in logarithmic scale) between the iterates and the flat minimizer for all runs of the specified batch size and specified learning rate.

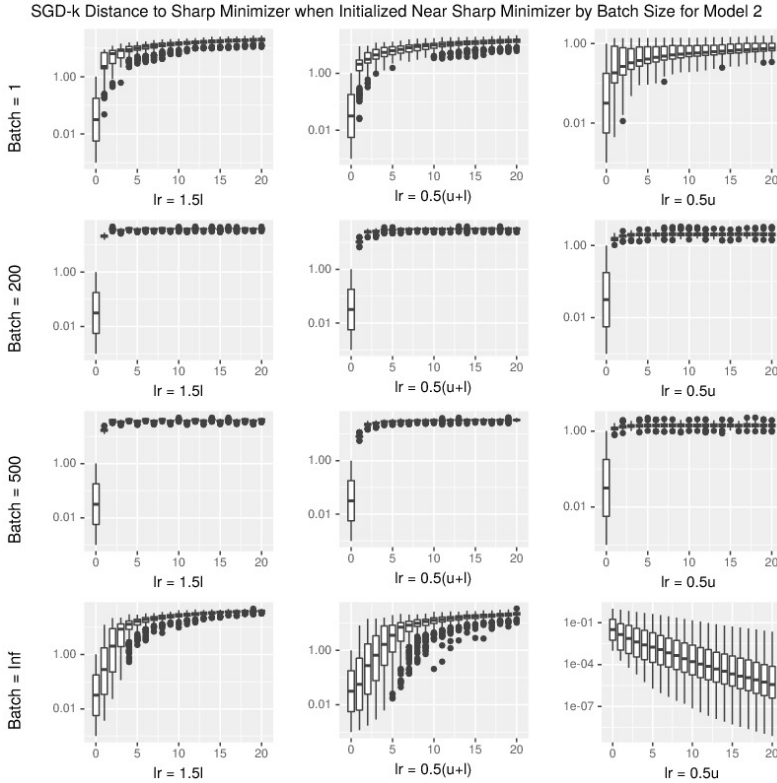


FIG. 17. The behavior of SGD-k on Model 2 for different batch sizes when initialized near the sharp minimizer. The y-axis shows the distance (in logarithmic scale) between the iterates and the sharp minimizer for all runs of the specified batch size and specified learning rate.

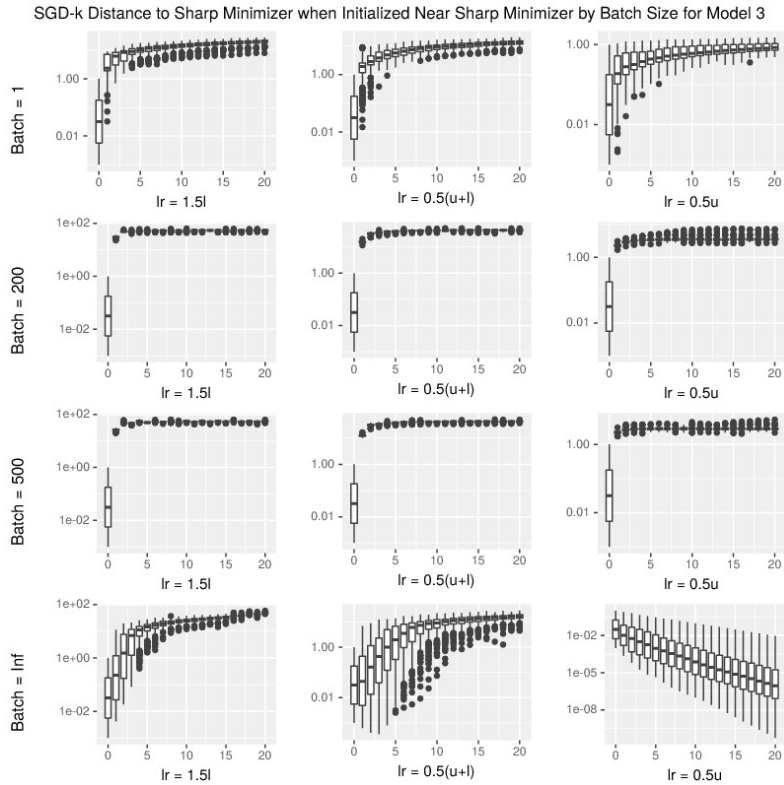


FIG. 18. The behavior of SGD-k on Model 3 for different batch sizes when initialized near the sharp minimizer. The y-axis shows the distance (in logarithmic scale) between the iterates and the sharp minimizer for all runs of the specified batch size and specified learning rate.

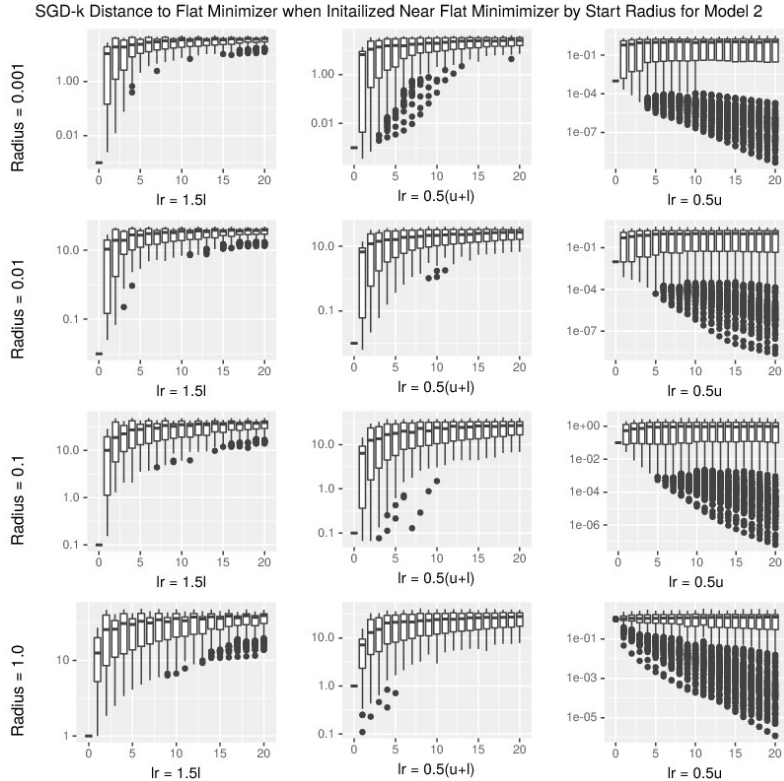


FIG. 19. The behavior of SGD-k on Model 2 for different starting radii when initialized near the flat minimizer. The y-axis shows the distance (in logarithmic scale) between the iterates and the flat minimizer for all runs of the specified starting radius and specified learning rate.

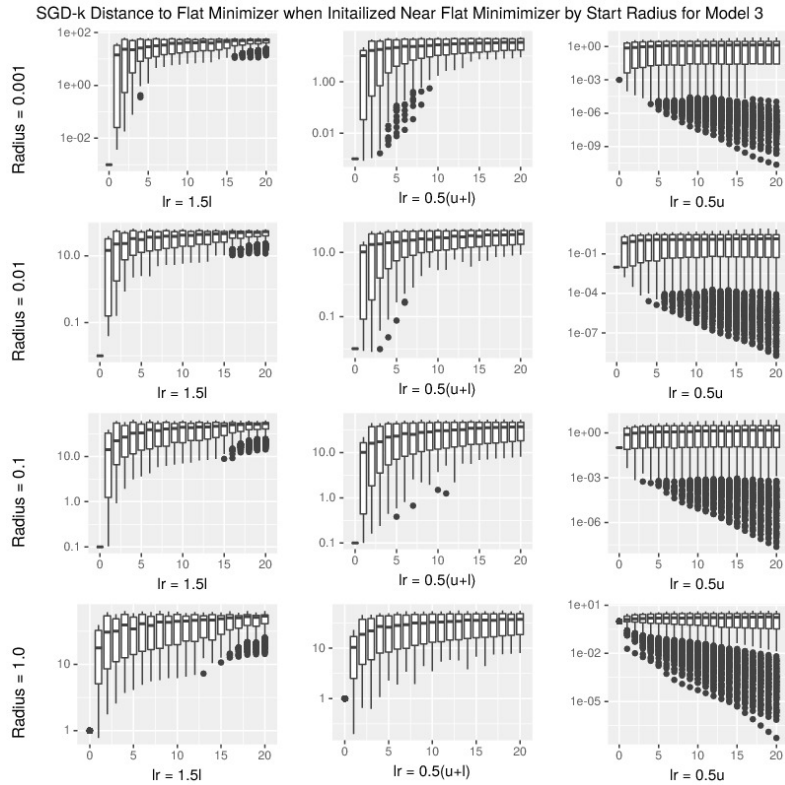


FIG. 20. The behavior of SGD-k on Model 3 for different starting radii when initialized near the flat minimizer. The y-axis shows the distance (in logarithmic scale) between the iterates and the flat minimizer for all runs of the specified starting radius and specified learning rate.

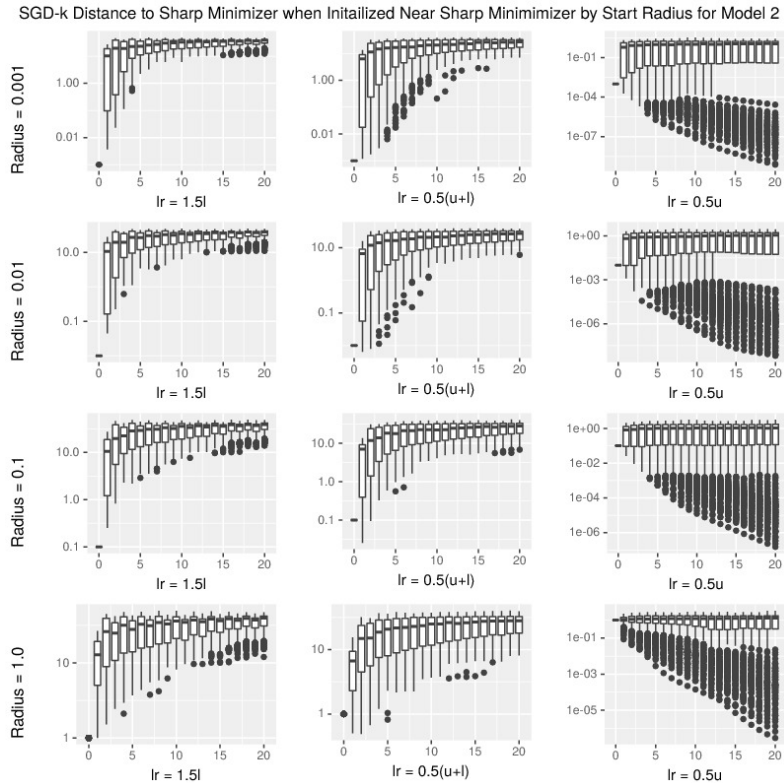


FIG. 21. The behavior of SGD-k on Model 2 for different starting radii when initialized near the sharp minimizer. The y-axis shows the distance (in logarithmic scale) between the iterates and the sharp minimizer for all runs of the specified starting radius and specified learning rate.

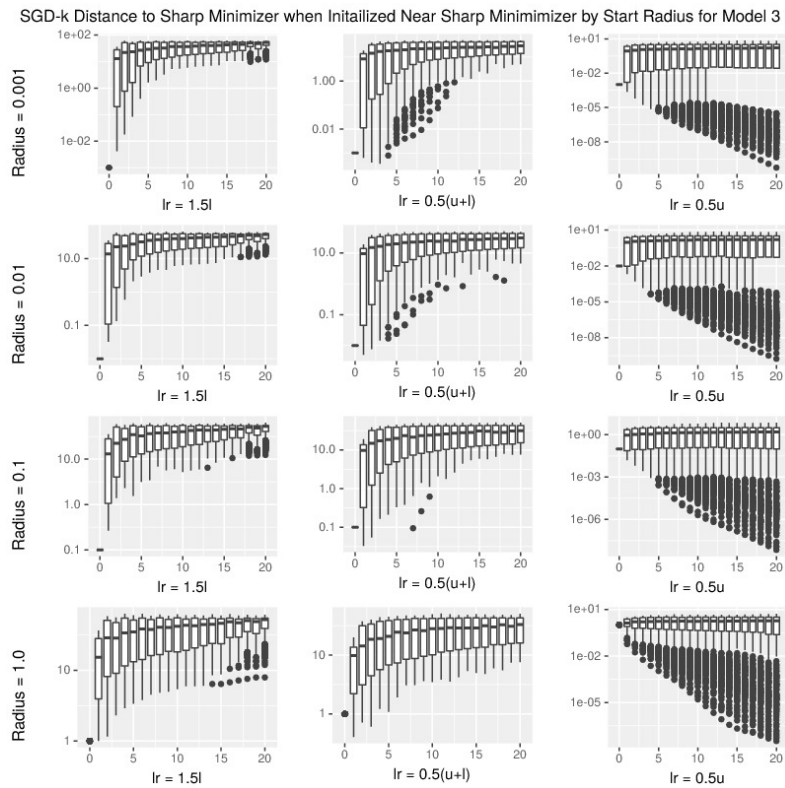


FIG. 22. The behavior of SGD-k on Model 3 for different starting radii when initialized near the sharp minimizer. The y-axis shows the distance (in logarithmic scale) between the iterates and the sharp minimizer for all runs of the specified starting radius and specified learning rate.